The *Card19* locus of murine chromosome 13 regulates terminal cell lysis downstream of caspase activation and Gasdermin-D cleavage

Card19 locus regulates caspase-dependent cell lysis

Elisabet Bjanes[1,2,#], Reyna Garcia Sillas[2], Rina Matsuda[1,2], Benjamin Demarco[3], Timothée Fettrelet[3], Alexandra A. DeLaney[1,2], Eric M. Rodriguez Lopez[2,4], Daniel Grubaugh[2], Meghan A. Wynosky-Dolfi[2,&], Naomi H. Philip[2,4,§], Elise Krespan[2,5], Dorothy Tovar[2,¶], Leonel Joannas[2,6], Daniel P. Beiting[2,5,7], Jorge Henao-Mejia[2,6,7], Brian C. Schaefer[8], Kaiwen W. Chen[3,%], Petr Broz[3], Igor E. Brodsky[2,7*]

[1]Cell and Molecular Biology Graduate Group, University of Pennsylvania Perelman School of Medicine, Philadelphia, Pennsylvania, United States of America
[2]Department of Pathobiology, University of Pennsylvania School of Veterinary Medicine, Philadelphia, Pennsylvania, United States of America
[3]Department of Biochemistry, University of Lausanne, Epalinges, Vaud, Switzerland
[4]Immunology Graduate Group, University of Pennsylvania Perelman School of Medicine, Philadelphia, Pennsylvania, United States of America
[5]Center for Host Microbial Interactions, University of Pennsylvania School of Veterinary Medicine, Philadelphia, Pennsylvania, United States of America
[6]CRISPR/Cas9 Mouse Targeting Core, University of Pennsylvania School of Veterinary Medicine, Philadelphia, Pennsylvania, United States of America
[7]Institute for Immunology, University of Pennsylvania Perelman School of Medicine, Philadelphia, Pennsylvania, United States of America
[8]Department of Microbiology and Immunology, Uniformed Services University, Bethesda, Maryland, United States of America

[#]Current address: Department of Pediatrics, University of California San Diego, La Jolla, California, United States of America
[&]Current address: Innate Immunity Research Unit, GlaxoSmithKline, Collegeville, Pennsylvania, United States of America
[§]Current address: Department of Immunobiology, Yale University School of Medicine, New Haven, Connecticut, United States of America
[¶]Current address: Department of Microbiology & Immunology, Stanford University School of Medicine, Palo Alto California, United States of America
[%]Current address: Immunology Programme and Department of Microbiology & Immunology, Yong Loo Lin School of Medicine, National University of Singapore, Singapore

*Correspondence to: ibrodsky@vet.upenn.edu

Author Contributions

Conceptualization: E.B., and I.E.B. Formal Analysis: R.M. Investigation: E.B., R.G.S., R.M., B.D., T.F. A.D, E.M.R.L, D.G., M.A.W-D., N.H.P., and D.T. Supervision: L.J., J.H-M., K.W.C., P.B., and I.E.B. Resources: L.J., D.B., E.K., B.C.S., J.H-M., and P.B. Funding Acquisition: I.E.B. Writing: E.B., B.C.S., K.W.C., I.E.B.

Abstract

Cell death plays a critical role in inflammatory responses. During pyroptosis, inflammatory caspases cleave Gasdermin D (GSDMD) to release an N-terminal fragment that generates plasma membrane pores that mediate cell lysis and IL-1 cytokine release. Terminal cell lysis and IL-1β release following caspase activation can be uncoupled in certain cell types or in response to particular stimuli, a state termed hyperactivation. However, the factors and mechanisms that regulate terminal cell lysis downstream of GSDMD cleavage remain poorly understood. In the course of studies to define regulation of pyroptosis during *Yersinia* infection, we identified a line of *Card19*$^{-/-}$ mice whose macrophages were protected from cell death and showed reduced pore formation during apoptosis or pyroptosis, yet had wild-type levels of caspase activation, IL-1 secretion, and GSDMD cleavage. Unexpectedly, CARD19, a mitochondrial CARD-containing protein, was not directly responsible for this, as two independently-generated CRISPR/Cas9 *Card19* knockout mice showed no defect in macrophage cell lysis. The original *Card19*$^{-/-}$ line was generated in a 129SvEvBrd background, and SNP analysis revealed a six megabase region of 129 origin co-segregating with the *Card19* locus. *Card19* is located on chromosome 13, adjacent to *Ninj1*, which was recently reported to regulate cell lysis downstream of GSDMD activation. Nonetheless, we could not detect major defects in NINJ1 protein expression or mutations in *Ninj1* coding sequence in *Card19*$^{-/-}$ mice. Mice from the original *Card19*$^{-/-}$ line exhibited significantly increased susceptibility to *Yersinia* infection, demonstrating that cell lysis itself plays a key role in protection against bacterial infection. Our findings identify a locus on murine chromosome 13 that regulates the ability of macrophages to undergo plasma membrane rupture downstream of gasdermin cleavage, and implicates additional NINJ1-independent factors that control terminal cell lysis.

Author Summary

Programmed cell death is critical for regulating tissue homeostasis and host defense against infection. Pyroptosis is an inflammatory form of programmed cell death that couples cell lysis with release of inflammatory cytokines. Cell lysis is triggered by activation of particular intracellular pore forming proteins, but how regulation of cell lysis occurs is not well understood. We identified the *Card19* locus on chromosome 13 as playing a key role in regulating terminal cell death in response to danger signals, such as bacterial infections or harmful chemicals. We found that immune cells from *Card19*$^{-/-}$ mice were resistant to multiple forms of cell death in response to a variety of harmful stimuli, including bacterial infections. *Card19*$^{-/-}$ mice were more susceptible to *Yersinia* infection, indicating that cell lysis contributes to control of bacterial infections. Our data provide new insight into the impact of terminal cell lysis on control of bacterial infection and indicate that additional factors exist that regulate lytic cell death.

Introduction

Regulated cell death is an evolutionarily conserved mechanism by which multicellular organisms regulate fundamental biological processes ranging from tissue development to control of microbial infection. Apoptosis and pyroptosis represent two distinct forms of regulated cell death that are activated in response to diverse stimuli, including developmental signals (1, 2), tissue stress or injury (3), and microbial infection (4-7). While apoptosis is an immunologically quiescent or suppressive form of cell death during tissue homeostasis and development, certain stimuli, including infections and chemotherapeutic agents, induce apoptosis that is accompanied by inflammatory signals that contribute to anti-pathogen and anti-tumor immunity (8-10). Apoptosis is activated by specific initiator apoptotic caspases, following certain intrinsic or extrinsic signals, and mediates organized disassembly of the cell via a process that limits cellular permeability and enables phagocytosis of the dying cell (11, 12). Alternatively, pyroptosis is a lytic form of regulated cell death characterized by caspase-1- or -11-dependent plasma membrane disruption mediated by cleavage and activation of the pore forming protein Gasdermin D (GSDMD), and release of interleukin-1 (IL-1) family cytokines and other intracellular components (13-16). However, inhibition of the receptor-proximal signaling kinases TAK1 or IKK by chemotherapeutic drugs or during infection by bacterial pathogens such as *Yersinia*, can trigger a caspase-8-dependent apoptosis pathway that is also associated with GSDMD cleavage (17-19). Interestingly, a recent study demonstrated that only caspase-8 activated in the RIPK1-containing complex IIb can efficiently cleave GSDMD in macrophages (20). These findings suggest a potential point of intersection of cell death pathways previously viewed as distinct (21).

During pyroptosis, secretion of IL-1 family cytokines and release of intracellular contents are temporally and genetically linked, and it has been suggested that IL-1 cytokines are released from cells when they undergo caspase-1 or -11-dependent lysis (22, 23). However, IL-1 secretion and cell lysis can be uncoupled in certain cell types or in response to specific stimuli. For example, the osmoprotectant glycine prevents release of lactate dehydrogenase (LDH), a key indicator of cell lysis, but does not affect IL-1β cytokine release (24, 25). Conversely, genetic ablation of IL-1 does not prevent cell lysis following pyroptotic stimuli. Moreover, IL-1 secretion can occur by living cells in the absence of apparent cytotoxicity (26, 27). Notably, neutrophils and monocytes display evidence of caspase-1 processing and IL-1 secretion in the absence of cell lysis (28, 29). Furthermore, dendritic cells treated with the oxidized lipid oxPAPC, or macrophages treated with the *N*-acetyl

glucosamine fragment of bacterial peptidoglycan, release IL-1 without undergoing cell death (30, 31). Interestingly, GSDMD is genetically required for the release of IL-1 cytokines in response to non-pyroptotic stimuli, a state termed hyperactivation (26, 31, 32). Collectively, these data imply that while GSDMD processing and membrane insertion are critical for ultimate cell lysis, a cell fate decision checkpoint exists that distinguishes GSDMD-dependent IL-1 secretion from terminal cell death.

In our efforts to identify regulators of cell death during bacterial infection, we investigated the caspase activation and recruitment domain (CARD)-containing protein CARD19 (33). CARD19 is a mitochondrial membrane protein that contains an N-terminal CARD and C-terminal transmembrane domain, suggesting that it could be involved in the regulation of cell death or inflammatory responses (33, 34). Multiple mitochondria-associated proteins regulate inflammasome activation and inflammatory signaling (35-37). Notably, the mitochondrial CARD-containing protein, MAVS, plays a critical role in anti-viral immune signaling and IL-1 cytokine release (35, 38), and the mitochondrial outer membrane lipid cardiolipin plays an important role in regulating NLRP3 inflammasome assembly (39).

Intriguingly, primary macrophages from *Card19*$^{-/-}$ mice were resistant to cell lysis and release of lytic cell markers in response to apoptotic and pyroptotic stimuli, but exhibited wild-type levels of caspase activation, IL-1 secretion, and gasdermin processing. Unexpectedly however, two independent CRISPR/Cas9 knockout mouse lines that we generated did not show the same phenotype; furthermore, expression of CARD19 in immortalized BMDMs from the original *Card19*$^{-/-}$ line did not restore their ability to undergo lysis, indicating that CARD19 itself was not responsible for regulating terminal cell lysis in response apoptotic and pyroptotic stimuli. Notably, the observed phenotypes were linked to a six megabase region in the *Card19* locus. RNA-seq identified a handful of differentially regulated genes in *Card19*$^{-/-}$ BMDMs, including a recently reported regulator of plasma membrane lysis, *Ninj1* (40), which is located adjacent to *Card19* on chromosome 13. Although *Card19*$^{-/-}$ BMDMs showed mildly reduced *Ninj1* mRNA expression at baseline, NINJ1 protein levels were unaffected both at baseline and upon LPS stimulation, indicating that the phenotype of *Card19*$^{-/-}$ mice is not due to a defect in NINJ1. Furthermore, the cell lysis defect in *Card19*$^{-/-}$ mice was also unrelated to the function of Sterile alpha and heat armadillo motif-containing protein (SARM1), which was reported to regulate NLRP3 inflammasome-dependent cell death independently of IL-1β cytokine release (41), as BMDMs from four independent *Sarm1*$^{-/-}$ lines showed no defects in cell death, IL-1β release, and GSDMD cleavage.

Allelic differences in inbred mouse lines or passenger mutations in linked genes have led to advances in understanding of innate immune signaling and antibacterial defense, such as the *Ity/Bcg/Lsh* locus (42, 43), the *Ltx/Nalp1b* locus (44), the spontaneous *Casp11* mutation in *Casp1/11* mice (23), and the *Lps* locus that distinguished LPS responsiveness in C3H/HeJ from C3H/HeN mice (45). Our findings identify a 6 MB region of chromosome 13 that impacts cell fate and anti-bacterial host defense downstream of GSDMD cleavage and implicate the existence of additional factors in the *Ninj1/Card19* locus that regulate plasma membrane rupture and cell lysis following caspase activation.

Results

Card19$^{-/-}$ BMDMs are deficient for caspase-dependent cell death

Our efforts to understand how cell death is regulated during bacterial infection led us to investigate the mitochondrial CARD-containing protein, CARD19, formerly known as BinCARD-2 (33, 34). To test the possible contribution of CARD19 to cell death during pyroptosis, we investigated the kinetics of cell death in B6 and *Card19*$^{-/-}$ primary bone marrow-derived macrophages (BMDMs) in response to infection by the pyroptotic stimuli *Salmonella enterica* serovar Typhimurium (*S*. Tm) or LPS+ATP. *S*. Tm infection of BMDMs induces the well-characterized NAIP/NLRC4/caspase-1 inflammasome pathway, leading to pyroptosis and IL-1 cytokine release (4, 5, 46, 47). In contrast, LPS+ATP treatment activates the NLRP3/ASC/caspase-1 inflammasome, which induces pyroptosis and IL-1 cytokine release via activation of the P2X7 receptor and potassium efflux (48-52). Intriguingly, *Card19*$^{-/-}$ BMDMs displayed a striking and significant defect in cell death following *S.* Tm infection or LPS+ATP treatment, as measured by release of LDH **(Fig. 1A and 1B)**. Consistently, *Card19*$^{-/-}$ BMDMs exhibited significantly reduced levels of membrane permeability, both in kinetics and amplitude **(Fig. 1C and 1D)**.

Card19$^{-/-}$ BMDMs also exhibited a significant defect in cell death following infection by *Yersinia pseudotuberculosis* (*Yp*), which activates cell-extrinsic caspase-8- and RIPK1-dependent apoptosis in response to *Yp* blockade of IKK- and MAPK-signaling (6, 53, 54), as well as in response to the broad-spectrum kinase inhibitor staurosporine (Sts), which induces cell-intrinsic apoptosis and also activates caspase-8 in myeloid cells (55-57) **(Fig. 1E and 1F**). These observations were also mirrored by delayed PI uptake in *Card19*$^{-/-}$ BMDMs **(Fig. 1G and 1H)**. Strikingly, *Card19*$^{-/-}$ BMDMs were similarly resistant to cell death in response to multiple apoptotic and pyroptotic stimuli, including cycloheximide, etoposide, and noncanonical inflammasome activation **(Fig. 2A-2C)**. However, RIPK3-dependent programmed necrosis which occurs in response to LPS and the pan-caspase

inhibitor z-VAD-FMK (58, 59), was unaffected by CARD19-deficiency **(Fig. 2D)**. Altogether, these findings demonstrate that BMDMs from *Card19*$^{-/-}$ mice exhibit increased resistance to membrane permeability and terminal cell lysis downstream of apoptotic and pyroptotic triggers.

Peritoneal macrophages from *Card19*$^{-/-}$ mice have reduced levels of cell death

The peritoneal cavity contains two distinct populations of macrophages, termed Large and Small (LPM and SPM, respectively)(60). At baseline, the primary population is the LPM, while 2 days post-injection of LPS or other inflammatory triggers, such as thioglycolate the primary population in the peritoneal cavity shifts to the SPM (60, 61). Interestingly, thioglycolate-elicited peritoneal macrophages exhibited significantly higher levels of LDH than peritoneal macrophages isolated from PBS-treated mice following infection with either *S.*Tm or *Yp* **(Fig. 3A-3C)**. These data indicate that SPM undergo elevated levels of cell death relative to LPMs. Moreover, thioglycolate-elicited PMs from *Card19*$^{-/-}$ mice had significantly lower levels of LDH release that C57BL/6J PMs, indicating that macrophages from *Card19*$^{-/-}$ animals have a general defect in cell lysis **(Fig. 3D and 3E)**.

***Card19*$^{-/-}$ BMDMs retain intracellular alarmin HMGB1 following activation of cell death**

HMGB1 is a nuclear chromatin-associated protein that is released from cells upon loss of plasma membrane integrity (62). As expected in B6 cells, *S*. Tm or LPS+ATP treatment led to significant HMGB1 release into the supernatant by one-hour post-infection, and by 4 hours post-exposure to *Yp* or staurosporine (Sts) **(Fig. 4A)**. In contrast, *Card19*$^{-/-}$ cells exhibited significantly delayed release of HMGB1 for each respective timepoint, consistent with our findings that they exhibit increased resistance to membrane rupture **(Fig. 4A)**. HMGB1 was virtually undetectable in *Card19*$^{-/-}$macrophage supernatants one-hour post-treatment with *S*. Tm or LPS+ATP, and minimally detectable at 4 hours post-treatment in response to *Yp* or Sts **(Fig. 4A)**. To obtain insight into the dynamics of HMGB1 release from cells, we analyzed HMGB1 release by confocal microscopy following exposure of Wt and *Card19*$^{-/-}$ cells to Sts. We observed three morphologies of HMGB1 staining – nuclear, in which the majority of HMGB1 was located in the nucleus; cellular, in which HMGB1 was absent from the nucleus but still contained within the confines of a cell; and extracellular, in which a cloud of HMGB1 was detectable surrounding what was likely the remnants of apoptotic cells and cellular debris. Notably, and consistent with intracellular retention of HMGB1 in *Card19*$^{-/-}$ cells, a higher frequency of *Card19*$^{-/-}$ cells relative to B6 BMDMs retained nuclear HMGB1 **(Fig. 4B and 4C)**, while B6 BMDMs exhibited extracellular HMGB1 cloud formation much more frequently than *Card19*$^{-/-}$ BMDMs **(Fig. 4B white arrows and quantified in Fig. 4D)**. Altogether, these findings

indicate that *Card19*$^{-/-}$ BMDMs resist cell lysis and release of intracellular contents during induction of cell death triggered by caspase-1 or caspase-8.

Card19$^{-/-}$ macrophages are not deficient in activation of caspase-1 or -8

Most currently known regulators of cell death act at the level of caspase activation or assembly of caspase-activating inflammasome complexes (63). Pyroptosis is mediated by activation of caspase-1 or -11 (15, 63, 64), which cleave Gasdermin D (GSDMD), thereby triggering cell lysis by enabling formation of oligomeric N-terminal GSDMD pores in the plasma membrane (14, 16, 65, 66). Surprisingly, despite the significant reduction in cytotoxicity in *Card19*$^{-/-}$ cells, processing of caspase-1 was equivalent in B6 and *Card19*$^{-/-}$ cells 15 minutes post-infection, at which time cell death is virtually undetectable in either genotype **(Fig. 5A)**. Moreover, B6 cells released significant amounts of cleaved and pro-caspase-1 into cell supernatants at later timepoints, in contrast to *Card19*$^{-/-}$ BMDMs **(Fig. 5A)**, consistent with the reduced levels of pyroptosis in *Card19*$^{-/-}$ cells in response to *S*. Tm infection. Reduced levels of cleaved caspase-1 in *Card19*$^{-/-}$ BMDM supernatants was matched by increased amounts of cleaved caspase-1 in *Card19*$^{-/-}$ whole cell lysates **(Fig. 5A)**. Similarly, initial processing of GSDMD to the cleaved p30 form was equivalent in B6 and *Card19*$^{-/-}$ cell lysates, while the release of processed GSDMD into the supernatant was significantly reduced in *Card19*$^{-/-}$ cells **(Fig. 5A)**. Thus, *Card19*$^{-/-}$ cells have no defect in either caspase-1 activation, or in the cleavage of caspase-1 targets.

Cell-extrinsic apoptosis is mediated by oligomerization and auto-processing of caspase-8 (67, 68). Active caspase-8 directly cleaves its pro-apoptotic downstream targets, including the Bcl-2 family member Bid (69, 70), and the executioner caspases-3 and -7. Similarly to caspase-1, cleavage of caspase-8 as well as the processing of caspase-8 substrates, including Bid, caspase-3, the caspase-3 target poly-ADP ribose polymerase (PARP), and the pore-forming protein GSDME also known as DFNA5 (18, 71), were equivalent in B6 and *Card19*$^{-/-}$ cells in response to *Yp* infection or staurosporine treatment **(Fig. 5B and 5C)**. Notably, we observed GSDMD processing in response to *Yp* infection as well as Sts treatment, in both B6 and *Card19*$^{-/-}$ BMDMs **(Fig. 5C)**. Importantly, direct comparison of caspase-1 and GSDMD processing in response to multiple stimuli revealed that *Card19*$^{-/-}$ cells had reduced release of cleaved caspase-1 and N-terminal GSDMD into the supernatant, and correspondingly increased retention in cell lysates, consistent with reduced terminal lysis of the cells in the absence of CARD19 **(Fig. 5D)**. *Card19*$^{-/-}$ BMDMs had wild-type levels of caspase-8 activity in response to either *Yp* infection or Sts treatment, confirming that *Card19*$^{-/-}$ BMDM do not have a defect in caspase activity **(Fig. 5E)**.

Altogether, these findings demonstrate that *Card19*$^{-/-}$ BMDMs do not have a defect in caspase activation or downstream target cleavage, and therefore likely have a defect in cell lysis downstream of caspase activation.

How *Card19*$^{-/-}$ cells might retain membrane integrity downstream of both inflammatory and apoptotic caspase activation is not clear. However, caspase-8 and caspase-1 can both cleave IL-1β (55, 72, 73), as well as GSDMD (17, 18, 20) raising the question of whether *Card19*$^{-/-}$ cells and *Gsdmd*$^{-/-}$ cells have similar defects in cell lysis in response to *Yp* infection. Surprisingly, although *Gsdmd*$^{-/-}$ BMDMs exhibited a significant defect in cell death in response to *Yp* infection **(Fig. S1A)**, this defect was not as pronounced as in *Card19*$^{-/-}$ BMDMs, suggesting that *Card19*$^{-/-}$ cells likely have a defect in additional GSDMD-independent mechanisms of cell lysis, potentially involving GSDME/DFNA5, which was also processed in response to *Yp* infection **(Fig. S1B and S1C)**. Consistent with recent findings (17-19), we observed cleaved GSDMD in *Casp1/11*$^{-/-}$ lysates following either *Yp* infection or staurosporine treatment. Although levels of cleaved GSDMD were significantly lower than in Wt cells, this finding is consistent with findings that caspase-8 cleaves GSDMD less efficiently than caspase-1 **(Fig. S1B and S1C) (19)**. The caspase-8-selective inhibitor, IETD, abrogated GSDMD and GSDME cleavage in response to *Yp* or staurosporine **(Fig. S1B and S1C)**, suggesting that *Yersinia* and staurosporine induce GSDMD and GSDME cleavage in *Casp1/11*$^{-/-}$ cells in a caspase-8-dependent manner. Consistently, *Ripk3*$^{-/-}$ BMDMs showed robust cleavage of GSDMD and GSMDE while *Ripk3*$^{-/-}$*Casp8*$^{-/-}$ BMDMs showed a near-complete absence of N-terminal GSDMD and GSDME p30 following *Yp* infection and significant reduction in GSDMD and GSDME processing after staurosporine treatment **(Fig. S1B and S1C)**. Notably, caspase-1 activity was not defective in the *Ripk3*$^{-/-}$*Casp8*$^{-/-}$ BMDMs **(Fig. S1D)**.

The cell death defect in *Card19*$^{-/-}$ BMDMs is independent from cytokine release

Consistent with our findings that *Card19*$^{-/-}$ BMDMs are not defective in their ability to regulate proteolytic activity of caspase-1, CARD19-deficient cells released wild-type levels of IL-1 cytokines in response to *S*. Tm, LPS+ATP, or infection with the Δ*yopEJK Yp* strain, which triggers a caspase-11/NLRP3-dependent pathway of IL-1 cytokine release (74, 75) **(Fig. 6A, B)**. These data indicate that *Card19*$^{-/-}$ cells most likely do not have a defect at the level of GSDMD-dependent pore formation and cytokine release and that the *Card19*$^{-/-}$ cells decouples secretion of IL-1β from pyroptosis, which normally occurs in response to these stimuli (26, 32). Consistent with a recent finding that *Card19*$^{-/-}$ cells do not have altered NF-κB activation (33), *Card19*$^{-/-}$ BMDMs did not have a defect in secretion of IL-6, TNF, or IL-12p40, **(Fig. 6C-6E)**. Altogether, these findings suggest that

Card19$^{-/-}$ cells have decoupled cell lysis as determined by LDH and HMGB1 release and the release of caspase-1-dependent cytokines.

Cells can release IL-1β while remaining viable during a state known as hyperactivation (26, 32, 76). GSDMD is required for IL-1β secretion during hyperactivation, but the mechanism by which GSDMD mediates this IL-1β released without inducing lysis is not understood (26, 76). *Staphylococcus aureus* lacking OatA induces hyperactivation (26, 76). Despite inducing robust IL-1β release under conditions of minimal LDH release, Δ*oatA S. aureus*-infected B6 BMDM exhibited minimal levels of caspase-1 and GSDMD processing **(Fig 6F-6H)**. CARD19 expression did not correlate with differences in hyperactivation exhibited between untreated, Δ*oatA* and *S.* Tm-infected BMDMs **(Fig. 6F)**. Since *Card19*$^{-/-}$ BMDMs process caspase-1 and GSDMD normally while releasing IL-1 cytokines in the absence of overt lysis, these data indicate that lack of death in *Card19*$^{-/-}$ cells is not evidence of a hyperactivation phenotype, but are likely resistant to cell lysis due to a defect at a terminal stage of pyroptosis. Curiously, Δ*oatA*-infected cells exhibited significantly lower levels of GSDMD processing, indicating that threshold levels of GSDMD processing or membrane insertion may underlie the distinction between hyperactivation and cell lysis **(Fig. 6F)**.

Card19$^{-/-}$ mice exhibit increased susceptibility to *Yersinia*

We next assessed whether the impact of CARD19 on cell death was biologically relevant during an *in vivo* infection in which cell death is essential for systemic bacterial control. Consistent with findings that mice lacking essential mediators of cell death are more susceptible to bacterial infection (53, 77-79), *Card19*$^{-/-}$ mice were more susceptible to oral *Yp* infection and had a defect in controlling systemic *Yp* tissue burdens **(Fig. 7A and 7B)**. *Yp*-infected *Card19*$^{-/-}$ mice exhibited increased splenomegaly **(Fig. 7C and 7D)**, suggesting either failure to control infection and elevated recruitment of inflammatory cells to the spleen, or a failure of innate cells to undergo cell death during bacterial infection in vivo. *Card19*$^{-/-}$ mice had similar levels of serum IL-6 and IL-12, although they had increased levels of TNF **(Fig. 7E)**, consistent with increased bacterial burdens *in vivo* and the finding that CARD19 itself is not required for cell-intrinsic inflammatory cytokine production. Altogether these data indicated that CARD19 is not important for control of cell-intrinsic cytokine production but contributes to host defense against bacterial infection.

Card19$^{-/-}$ BMDMs regulate cell lysis independently of SARM1 or NINJ1

Numerous mitochondrial proteins have been implicated in recent years as essential regulators of caspase activity, GSDMD and terminal events in during lysis (35, 37, 80). While these studies were in progress, Sterile alpha and armadillo motif-containing protein (SARM1) was found to regulate terminal cell lysis following stimulation of the NLRP3 inflammasome (41), and like CARD19, also localizes to the mitochondrial outer membrane (33). Unexpectedly however, BMDMs isolated from multiple independent lines of *Sarm1*$^{-/-}$ mice (described further in Materials and Methods), including the *Sarm1*$^{-/-}$ mice reported in the Carty *et al*. study (41), originally described by Kim et al (81), did not exhibit any defects in their ability to undergo cell lysis in response to canonical NLRP3 inflammasome stimuli **(Fig. S2A)**, nor did they exhibit elevated levels of inflammasome-dependent IL-1β release **(Fig. S2B).** *Sarm1*$^{-/-}$ BMDMs also showed wild-type levels of Caspase-1, GSDMD, and IL-1β processing **(Fig. S2C and S2D)**. Moreover, TNF release was unaffected in cells lacking SARM1 compared to WT controls, indicating that the NLRP3 inflammasome priming step (NF-κB pathway) is not dysregulated by the absence of SARM1 (**Fig. S2E**). Furthermore, in contrast to *Card19*$^{-/-}$ BMDMs, the *Sarm1*$^{-/-}$ macrophage lines had wild-type levels of cell death and cytokine release in response to non-canonical inflammasome activation **(Fig. S2F and S2G)**. Notably, some *Sarm1*$^{-/-}$ lines were reported to contain a passenger mutation in the closely-linked gene *Xaf1*, indicating that some previous cell death-related phenotypes attributed to SARM1 may be due to alteration of *Xaf1* (82). Altogether, these findings indicate that the phenotype of *Card19*$^{-/-}$ BMDMs is not related to potential interactions with SARM1.

Next, to test the sufficiency of CARD19 to induce cell death, we generated immortalized *Card19*$^{+/+}$ and *Card19*$^{-/-}$ bone marrow hematopoietic progenitors using the ER-HOXB8 system (83), and transduced the progenitors with CARD19-expressing lentiviral constructs. Unexpectedly, *Card19*$^{-/-}$ iBMDMs transduced with CARD19 displayed comparable death to vector control-transduced iBMDMs, raising questions as to whether CARD19-deficiency was directly responsible for the observed defect in caspase-dependent death in *Card19*$^{-/-}$ BMDMs **(Fig. 8A)**.

Passenger mutations in genes closely linked with the gene of interest in backcrossed C57BL/6 mice can confound interpretation of immune responses and cell death pathways in these lines (23, 84, 85). Notably, *Card19*$^{-/-}$ mice were originally generated using 129SvEvBrd ESCs, and backcrossed for 10-12 generations (33). SNP genotyping analysis of the *Card19*$^{-/-}$ mice indicated that approximately six megabases adjacent to the

Card19 locus were derived from the 129SvEvBrd lineage **(Fig. S3A, Table S2)**. *Card19*$^{+/-}$ and 129/SvIm/J BMDMs phenocopy wildtype BMDMs with respect to their ability to undergo terminal cell lysis in response to *S.* Tm., *Yp*, and Sts, indicating that the phenotype is linked to the *Card19* locus **(Fig. 8B-8D)**. To rule in or rule out the possibility that a passenger mutation linked to the *Card19* locus might be responsible, we next generated two independent *Card19*-deficient murine lines directly on the C57BL/6J background using CRIPSR/Cas9. The first of these removed exons 2-3, removing the entire CARD domain, but leaving a truncated mRNA that could produce a peptide fragment containing the transmembrane domain, which we termed *Card19*$^{\Delta CARD}$ **(Figure S3B, Table S1)**. The second was a complete deletion of the *Card19* locus, which we termed *Card19*^{Null} (see Methods for further details of construction of these lines). Critically, *Card19*$^{\Delta CARD}$ and *Card19*^{Null} BMDMs exhibited no observable defect in their ability to undergo cell lysis following infection with either *Yp* or treatment with LPS+ATP, in contrast to BMDMs derived from the original *Card19*$^{-/-}$ line **(Fig. 8E and 8F)**. Altogether, these data indicate that loss of CARD19 is not the mechanistic basis of the defect in cell death seen in the original *Card19*$^{-/-}$ cells.

To address the possibility that *Card19*$^{-/-}$ mice contain a functionally important polymorphism or have an expression defect in a gene closely linked to Card19, we performed whole exome sequencing on B6 and *Card19*$^{-/-}$ mice, and while we identified potential mutations in eight genes on chromosome 13, they were not high probability candidates **(Table S3)**. We further performed RNA-seq on B6 and *Card19*$^{-/-}$ BMDMs, with the hypothesis that transcriptional alteration of genes closely linked to *Card19*$^{-/-}$ might result in the observed loss of cell lysis **(Fig. 8G, Table S4)**. Intriguingly, *Ninj1*, recently identified as a key regulator of plasma membrane rupture during lytic cell death in response to apoptotic, pyroptotic and necrotic stimuli (40) is directly upstream of *Card19*, making it a possible candidate for passenger mutations **(Fig. S3A, blue arrow)**. *Card19*$^{-/-}$ and *Ninj1*$^{-/-}$ BMDMs have a strikingly similar phenotype, as they both have a defect in cell death that is independent of IL-1 cytokine release and processing of caspases and gasdermins ((40), **Fig. 1-5**). SNP mapping with a high density SNP array identified a 129SvEvBrd-derived region in *Card19*$^{-/-}$ cells downstream of both *Ninj1* and *Card19* that also contained several B6 SNPs (**Table S2, Fig. S3A**). It is therefore likely that complex recombination occurred at the *Ninj1/Card19* locus **(Fig. S3A, Table S2)**. To test whether any mutations in *Ninj1* were present in the *Card19*$^{-/-}$ mice, we directly sequenced all 5 exons of *Ninj1*, including the 3' splice acceptor site for exon 2, reported to be mutated in the ENU-mutagenesis screen that first identified *Ninj1,* but were not able to detect any

deviations from the reference genome in the *Ninj1* sequence in *Card19*$^{-/-}$ mice. Furthermore, while *Ninj1* mRNA levels were reduced at baseline in *Card19*$^{-/-}$ BMDMs relative to wild-type BMDMs, NINJ1 protein levels were indistinguishable between wild-type and *Card19*$^{-/-}$ BMDMs **(Fig. 8G and 8H)**. Altogether, our findings indicate the presence of an additional key regulator of terminal cell lysis downstream of caspase activation and gasdermin processing, and suggest that this factor is located close to the *Ninj1-Card19* locus on chromosome 13.

Discussion

Our study has revealed that *Card19*$^{-/-}$ BMDMs are resistant to cell lysis during both pyroptosis and caspase-8-mediated apoptosis while maintaining caspase activation and release of IL-1 family cytokines. This data highlights the existence of a regulatory checkpoint downstream of gasdermin processing that controls the cell fate choice to undergo terminal cell lysis. Until relatively recently, caspase-dependent cleavage of gasdermin D, and the subsequent release of the gasdermin D N-terminal pore-forming domain was viewed as the terminal step in lytic cell death. However, certain cell types or stimuli can trigger IL-1β release without cell lysis (28, 29, 31, 86). The finding that gasdermin-dependent secretion of IL-1 cytokines can be uncoupled from cell lysis points to regulatory steps subsequent to cleavage and activation of gasdermin D that can be engaged to promote or limit cell lysis.

Our initial observations that *Card19*$^{-/-}$ macrophages were resistant to cell lysis despite having wild-type levels of GSDMD processing suggested that CARD19 might play an important role in this process. Nonetheless, two CRISPR/Cas9-generated lines of mice made directly on a B6 background (*Card19*$^{\Delta CARD}$ and *Card19*^{Null}) did not recapitulate this phenotype, nor were we able to restore the lysis phenotype in *Card19*$^{-/-}$ cells by expressing CARD19. These findings point to a CARD19-independent factor as being responsible for the resistance of *Card19*$^{-/-}$ cells to cell lysis. Intriguingly, *Ninj1* which is immediately upstream of *Card19* on chromosome 13, is a regulator of cell lysis in response to pyroptotic, apoptotic, and necrotic stimuli (40). *Ninj1* encodes a protein whose function was previously linked to axonal guidance, and was identified in a forward genetic screen for regulators of cell death (40). The phenotype of *Ninj1*$^{-/-}$ cells is strikingly similar to that of *Card19*$^{-/-}$ BMDMs (40). However, *Card19*$^{-/-}$ BMDMs have WT levels of NINJ1 protein expression, and we were unable to identify any mutations in the NINJ1 coding sequence or intronic splice acceptor that would indicate a potential defect in NINJ1 in *Card19*$^{-/-}$ mice. Moreover, whereas *Ninj1*$^{-/-}$ BMDMs have defects in their ability to undergo cell lysis downstream of necroptosis as well as pyroptosis, *Card19*$^{-/-}$ BMDMs were unaffected in their ability to undergo

LDH release during necroptosis. While it remains possible that *Card19*$^{-/-}$ mice have a cryptic defect in *Ninj1* that arose spontaneously or as a result of *Card19* gene targeting, our data support the existence of additional factor(s) in this locus that regulate cell lysis in response to caspase activation.

In addition to the finding by Kayagaki and colleagues that NINJ1 regulates cell lysis, Evavold *et al*. recently uncovered the Ragulator/Rag/mTORC pathway in a genetic screen for factors required in GSDMD-dependent pore formation (87). Intriguingly, the Ragulator complex acts downstream of GSDMD but upstream of NINJ1-induced cell lysis, as Rag was required for pore formation, whereas NINJ1 acts subsequent to pore formation to induce membrane rupture and ultimate cytolysis (40, 87). As *Card19*$^{-/-}$ macrophages exhibit a kinetic delay and reduced overall amplitude of pore formation, our findings suggest that the factor responsible acts at a similar step to the Ragulator complex, and upstream of NINJ1 to facilitate pore formation prior to terminal cell lysis. Thus, in contrast to previous models whereby release of the N-terminal portion of GSDMD was necessary and sufficient to trigger cell lysis, these findings collectively support a multi-step regulated process, downstream of GSDMD cleavage, that ultimately triggers lytic rupture of the cell.

How terminal cell lysis occurs downstream of GSDMD cleavage or plasma membrane insertion remains enigmatic. Interestingly, the mitochondrial protein SARM1 was found to regulate cell lysis in response to NLRP3 inflammasome activation independently of IL-1β cytokine release. Mitochondrial disruption is a feature of both lytic and apoptotic forms of cell death, and the N-terminal GSDMD fragment is recruited to the mitochondrial membrane as well (80, 88). However, in our hands, primary macrophages generated from four independent lines of *Sarm1*$^{-/-}$ BMDMs had wild-type levels of cell lysis and IL-1β cytokine release. Whether passenger mutations, which have been reported in *Sarm1*$^{-/-}$ murine lines (82), may account for the reported phenotype of *Sarm1*$^{-/-}$ BMDMs, remains to be determined. Precisely how cell lysis can be uncoupled from IL-1 cytokine release remains a key unanswered question in this field. BMDMs from *Card19*$^{-/-}$, *Ninj1*$^{-/-}$, and *Rag*$^{-/-}$ all display reduced cell lysis despite substantial levels of IL-1β cytokine release, similar to the hyperactivation phenotype previously described by Kagan and colleagues (26). However, we observed that cells induced to undergo hyperactivation following infection with Δ*oatA* mutant *S. aureus* exhibit reduced levels of total caspase-1 and GSDMD cleavage, suggesting that the regulated step in hyperactivation occurs at the level of caspase processing or complex assembly, rather than at the level of GSDMD pore formation.

In addition to revealing the likely presence of additional factors that regulate terminal cell lysis in the setting of caspase activation, this study extends our understanding of the role lytic cell death plays in antibacterial host defense. *Card19*$^{-/-}$ mice showed significantly increased susceptibility to *Yersinia* infection, with higher systemic burdens and reduced ability to survive infection, consistent with our previous studies demonstrating that the RIPK1-Casp8-dependent cell death pathway was necessary for activation of cytokine production by uninfected bystander cells, our recently published and current work supports an immunological framework in which lytic cell death is one of many contributors to *in vivo* defense against bacterial infection.

While we do not know the factor responsible for resistance to cell lysis in the original *Card19*$^{-/-}$ mouse line, the evidence points to close linkage with the *Card19* locus. First, the phenotype of *Card19*$^{-/-}$ BMDMs has persisted across multiple back-crossed generations from N4 to N12. Second, BMDMs from numerous independent *Card19*$^{+/-}$ BMDMs exhibit wild-type phenotypes, indicating that homozygosity at the *Card19* locus is required for the phenotype. Third, SNP analysis reveals only a 6MB region adjacent to *Card19* as being derived from the 129SvEvBrd ES cells used to generate the original *Card19*$^{-/-}$ line (33). While it is possible that disruption of *Card19* in this line also inadvertently impacts NINJ1 expression, our RNA-seq and western blot analyses indicate minimal, if any, impact on *Ninj1* mRNA and protein levels in *Card19*$^{-/-}$ BMDMs. A number of important immune signaling and host-defense factors were initially revealed by genetic methods in inbred lines of mice or due to the presence of spontaneous passenger mutations. Notably, the *Ity/Bcg/Lsh* locus responsible for resistance to *Salmonella, Mycobacterium,* and *Leishmania,* the *Ltx* locus responsible for differential resistance to Anthrax lethal toxin, and the *Lps* locus responsible for differential sensitivity to LPS-induced endotoxemia were initially defined via genetic approaches in inbred mouse lines (42-45, 89). Our findings point to a mutation within the *Card19/Ninj1* locus that disrupts the ability of murine macrophages to undergo plasma membrane rupture downstream of gasdermin cleavage, and indicate that additional factors beyond NINJ1 and the Ragulator/mTORC1 complex regulate terminal cell lysis.

Acknowledgements

We thank Sunny Shin, Jess Doerner, and Daniel Sorobetea for editorial suggestions, and members of the Shin and Brodsky labs for scientific discussion. We thank Russell Vance and Isabella Rauch (UC Berkeley) for *Gsdmd*$^{-/-}$ bone marrow. We thank Adriano Aguzzi (University Hospital Zurich) for providing the *Sarm1*$^{-/-}$ mice (*Sarm1(MSD)*) and Adolfo Garcia-Sastre (Icahn School of Medicine at Mount Sinai) for providing SARM1 knockout bone marrow (*SARM1(AGS)* and *SARM1(AD)*) including wild-type controls. We thank David Sykes (Harvard University) for providing us with ER-HoxB8 reagents. **Funding:** This work was supported by NIH grants AI125924, AI128530, and the Burroughs Wellcome Fund Investigator in the Pathogenesis of Infectious Disease award to I.E.B. **Competing Interests:** The authors declare no competing interests. **Data and materials:** Anti-caspase-1 antibody and *Ripk3*$^{-/-}$ mice were provided by Dr. Vishva Dixit (Genetech). *Gsdmd*$^{-/-}$ mice were provided by Dr. Russell Vance (University of California, Berkeley). Requests for resources and reagents should be directed to Igor E. Brodsky (ibrodsky@vet.upenn.edu).

Materials and Methods

All reagents and resources are listed in Table S5.

Generation of Card19$^{\Delta CARD}$ mice

Card19$^{\Delta CARD}$ mice were produced by the CRISPR/Cas9 Mouse Targeting Core (PSOM-UPenn) using CRISPR/Cas9 technology (flanking sgRNA and Cas9mRA microinjected in 1-cell mouse embryos), and a targeting strategy resulting in removal of exons 2-3. The resulting CARD19 deletion removes amino acids XX including the entire CARD and giving a predicted protein product of 87 AA in length.
CARD19 5' Target Sequence: GAGATACTGGTGGGACCGAAGGG.
CARD19 3' Target Sequence: TTGGTCACACTTCGCTGAGATGG.
Mice were backcrossed onto C57BL/6J for at least 2 consecutive generations.

Generation of *Card19^{Null}* mice

Card19^{Null} mice were produced by the CRISPR/Cas9 Mouse Targeting Core (PSOM-UPenn) using CRISPR/Cas9 technology (flanking sgRNA and Cas9mRA microinjected in 1-cell mouse embryos), and a targeting strategy resulting in deletion of exon 1, resulting in the premature appearance of a stop codon and degradation by nonsense-mediated decay.
CARD19 5' Target Sequence: TAGGCGAAGGGACGCCGACCCGG.
CARD19 3' Target Sequence: GTTTCTGGTACGAGCTGGCAGGG.
Mice were backcrossed onto C57BL/6J for at least 2 consecutive generations.

Differentiation of murine bone marrow-derived macrophages (BMDMs)

Bone marrow derived macrophages were isolated and differentiated as previously described (90). Briefly, isolated bone marrow cells from 6-10 week old male and female mice were grown at 37°C, 5% CO_2 in 30% macrophage media (30% L929 fibroblast supernatant, complete DMEM). BMDMs were harvested in cold PBS on day 7, and replated in 10% macrophage media onto tissue culture (TC)-treated plates and glass coverslips in TC-treated plates. *Sarm1(AGS3)$^{-/-}$*, *Sarm1(AGS12)$^{-/-}$*, and *Sarm1(AD)$^{-/-}$* were previously described and provided by Adolfo-Garcia Sastre (Icahn School of Medicine at Mount Sinai) along with wildtype controls (81, 82, 91).

Bacterial culture and infection conditions

Bacteria strains used include *Yersinia pseudotuberculosis* (*Yp*) strain IP2666, *Yp* ΔEJK (lacking Yop effector proteins YopE, YopJ, and YopK), *Salmonella enterica* serovar Typhimurium strain SL1344, *Shigella flexneri* M90T, DH5α *E. coli*, and Δ*oatA Staphylococcus aureus*. Bacterial strains were grown as previously described (26, 53, 75). Briefly, bacteria were grown with aeration and specific antibiotics at 28°C (*Yersinia*, irgasan) or 37°C (*Salmonella*, streptomycin, *E. coli*, none, *S. aureus*, kanamycin). *Shigella* was grown with aeration and without antibiotics at 37°C overnight in Tryptic Soy Broth. *Yersinia* strains were induced prior to infection by diluting the overnight culture 1:40 in 3 mL of inducing media (2xYT broth, 20 mM Sodium Oxalate, 20 mM $MgCl_2$). Inducing culture were grown at 28°C for 1 hour and shifted to 37°C for two hours with aeration. *Salmonella* strains were induced prior to infection by diluting the overnight culture 1:40 in 3 mL inducing media (LB broth, 300 mM NaCl), and grown standing for 3 hours at 37°C. Outgrowth cultures of *Shigella* were grown from overnight cultures for 2 hours at 37°C with aeration. Δ*oatA S. aureus* was grown overnight in Todd Hewitt Broth at 37°C with aeration (26). Bacterial growth was measured using OD_{600} on a spectrophotometer. Bacteria were pelleted, washed, and resuspended in DMEM or serum-free media for infection. *In vitro* infections were performed at MOI 10 (*Yp* and *S.* Tm., fractionation and microscopy), MOI 20 (*Yp, ΔEJK* and *S.* Tm., all other assays) or MOI 30 (*E. coli*, LDH) unless otherwise noted. Δ*oatA* infections were performed at MOI 30 and 60. Thioglycolate *in vitro* infections were performed at MOI 10. Gentamycin (100 μg/mL) was added one hour post infection for all infections.

Mouse strains

Card19$^{-/-}$ mice were previously described (33) and maintained as a breeding line in-house. B6 and *Casp1*/*Casp11$^{-/-}$* mice obtained from Jackson Laboratories and subsequently maintained as a breeding line in-house. All previously published knockout mouse lines that were used to generate BMDMs are indicated in Table S1. *Gsdmd$^{-/-}$* BMDMs were previously described (92), provided by Russell Vance, and maintained as a breeding line in-house. *Ripk3$^{-/-}$* mice (93) were a gift of Kim Newton and Vishva Dixit (Genentech) and *Ripk3/Casp8$^{-/-}$* mice (94) were a gift of Doug Green (St. Jude Children's Hospital). *Casp11$^{-/-}$* mice were originally generated by Junying

Yuan (95) (Harvard University) and kindly provided by Tiffany Horng (Harvard University). *Sarm1(MSD)*$^{-/-}$ mice were a gift from Adriano Aguzzi (University Hospital Zurich). Breeders were routinely genotyped. Mice were maintained in a specific pathogen-free facility by University Laboratory Animal Resources (ULAR) staff in compliance with IACUC approved protocols.

Generation of immortalized *Card19*$^{-/-}$ myeloid progenitors using ER-HOXB8

Card19$^{-/-}$ murine myeloid progenitors were immortalized using the ER-HoxB8 system (83). Bone marrow was harvested from female mice and myeloid progenitors were isolated using a Percoll density gradient. Progenitors were plated in 5% SCF-conditioned media supplemented with 10 ng/mL IL-3 and IL-6 for three days. Progenitors were spinfected on fibronectin coated plates with ER-HoxB8 retrovirus in 25 ug/mL polybrene at 1000g for 90 minutes. Progenitors were supplemented with 0.5 uM estrogen and 10 ng/mL GM-CSF to induce macrophage progenitor differentiation. Progenitors were replated with fresh estrogen and GM-CSF for two days. Retrovirally infected cells were selected for with the addition of 1 mg/mL geneticin for 2-3 days. Progenitors were harvested and passaged until immortalization was confirmed by the death of all uninfected control cells. Mature macrophages were generated from immortalized progenitors by plating cells in 30% macrophage media and growing for 5-6 days. Cells were fed with additional macrophage media on day 3.

Transduction of *Card19*$^{-/-}$ immortalized progenitors

HEK293T cells were transfected using Lipofectamine 2000 with pCL-Eco retroviral packaging vector and MSCV2.2-CARD19 or empty vector (MSCV2.2). Successful transfection was confirmed by imaging under a widefield as MSCV contains IRES-GFP. *Card19*$^{-/-}$ ER-HoxB8 immortalized progenitors were spinfected with filtered viral supernatants from transfected HEK293T cells at 2500 RPM for 90 minutes. Transduced progenitors were transduced a second time the following day as before to increase infection efficiency. Progenitors were allowed to recover and proliferate prior to 2.5 ug/mL puromycin selection. A 95%+ pure population was isolated by flow cytometry sorting on GFP+. Mature macrophages were generated from immortalized, transduced progenitors by plating cells in 30% macrophage media and growing for 5-6 days, with additional media supplementation on day 3.

Plasmids and constructs

All constructs are listed in Table S1. pcDNA3.1/CARD19-FLAG was obtained from GenScript (Refseq NM_026738.2). CARD19 was amplified and inserted into MSCV2.2 using Gibson cloning. All constructs were confirmed by sequencing prior to experimentation.

Cell death assays – LDH & PI uptake

LDH. Triplicate wells of BMDMs were seeded in TC-treated 96 well plates. BMDMs were infected with indicated bacterial strains as indicated above. BMDMs were primed with 100 ng/mL LPS for 3 hours followed by 2.5 mM ATP treatment. BMDMs were treated with 10 uM staurosporine or 100 uM etoposide. BMDMs were pretreated with 100 uM zVAD(OMe)-FMK or 100 ug/mL cycloheximide for 1 hour before treatment with 100 ng/mL LPS. For non-canonical inflammasome cell death, BMDMs were primed with 400 ng/mL Pam3CSK4 for 3 hours and then infected with DH5α *E. coli*, MOI 30 for 16-20 hours. For osmoprotected cell death, 5 mM glycine was added at the time of infection. 100 ug/mL gentamycin was added one hour post treatment to all infectious experimental conditions. BMDMs were primed with LPS (100 ng/ml) for 4 hours and stimulated with nigericin (5 μM). BMDMs were primed with Pam3CSK4 (1 μg/ml) for 4 h and were transfected with 2 μg/ml E. coli O111:B4 LPS with Fugene HD. At indicated time points, plates were spun down at 250g and supernatants were harvested. Sups were combined with LDH substrate and buffer according to the manufacturer's instructions and incubated in the dark for 35 min. Plates were read on a spectrophotometer at 490 nm. Percent cytotoxicity was calculated by normalizing to maximal cell death (1% triton) and no cell death (untreated cells).

PI uptake. Propidium Iodide uptake was performed as previously described (26). Briefly, triplicate wells of BMDMs were seeded in TC-treated black-walled 96 well plates. BMDMs were infected or treated as described above in 50 uL HBSS plus 10% FBS. Propidium Iodide (2x, 10 uM) was added in 50 uL HBSS to each well and incubated for 5 minutes in the dark to allow for stabilization of the signal in the maximal cell death wells (1% triton). PI uptake was detected by fluorescence on a BioTek Synergy HT Multi-Detection Microplate Reader (540/25 excitation, 590/35 emission, sensitivity 35, integration time 1 sec) every 2.5 minutes (*S.* Tm., ATP) or every 10 minutes (*Yp*, Sts) for the indicated time points. Gentamycin (100 ug/mL) was added one hour post infection (*Yp*, Sts). Percent cytotoxicity was calculated as described above.

Confocal microscopy

BMDMs were seeded as described above, treated with staurosporine for indicated time points, fixed, permeabilized, and blocked. BMDMs were stained for HMGB1 (1:200) at 37°C for 1 hr, Alexa Fluor rabbit 488 (1:4000) at RT for 1 hr, and Hoechst and Phalloidin at RT for 30 min. Slides were imaged as described above, with a single z-plane taken per field. Percent nuclear HMGB1 was quantified by identifying total HMGB1 staining per cell and comparing the overlap with nuclear staining (Hoechst). 65-200 cells were analyzed per genotype and condition. Cloud analysis was completed by counting the number of HMGB1 clouds per field of view with 5-8 fields per condition.

Caspase 8 activity

BMDMs were seeded as described above in a white-walled 96 well plate and treated with *Yp* or Sts for the indicated times. Z-IETD-fmk (500 uM, SM Biochemicals) was added 1 hour prior to infection/treatment as a control to block caspase-8 activity. Caspase-8 activity was detected using Caspase-8 Glo (Promega) according to the manufacturer's instructions. Luminescence was read on a Gen5 plate reader.

Western blots

BMDMs were seeded in TC-treated 24 or 12 well plates. Necrostatin (60 uM, Nec-1) was used to inhibit RIPK1 activity for 1 hour prior to *Yp* infection. Following infection or treatment in serum-free media, supernatants were harvested and TCA precipitated. Briefly, supernatants were spun down to remove cell debris and TCA precipitated overnight at 4°C. Sups were spun down and washed with acetone. Remaining TCA was neutralized with Tris, and the pellet was resuspended in 5x sample buffer (125 mM Tris, 10% SDS, 50% glycerol, 0.06% bromophenol blue, 1% β-mercaptoethanol). BMDMs were lysed in lysis buffer (20 mM HEPES, 150 mM NaCl, 10% glycerol, 1% Triton X-100, 1mM EDTA, pH7.5) plus 1x complete protease inhibitor cocktail and 1x sample buffer (25 mM Tris, 2% SDS, 10% glycerol, 0.012% bromophenol blue, 0.2% β-mercaptoethanol). Lysates and supernatants were boiled and centrifuged at full speed for 5 minutes, and sups were run on 4-12% polyacrylamide gels and transferred to PVDF. Membranes were immunoblotted using the following primary antibodies: β-Actin (1:5000), Bid (1:500), CARD19 (1:500), Caspase 1 (1:360), Caspase 3 (1:1000), Caspase 8 (1:1000), GSDMD (1:1000), HMGB1 (1:1000), GSDME (1:500), PARP (1:1000), NINJ1, Tubulin, and IL-1β. Species specific HRP-conjugated secondary antibodies were used for each antibody (1:5000). Membranes were developed using Pierce ECL Plus and SuperSignal West Femto Maximum Sensitivity Substrate according to the manufacturer's instructions. Western blot time-courses were performed in parallel with cytotoxicity assays to accurately interpret protein release before and after overt cell death.

Cytokine release

Triplicate wells of BMDMs were seeded in TC-treated 48 well plates. All conditions except untreated were primed with 100 ng/mL LPS for 3 hrs or unless otherwise indicated. BMDMs were infected with bacterial strains or treated with 2.5 mM ATP. BMDMs were primed with LPS (100 ng/ml) for 4 hours and stimulated with nigericin (5 μM). IL-1β release were measured at the indicated time points. BMDMs were primed with LPS (100 ng/ml) and TNF release was measured after 4 hours. BMDMs were primed with Pam3CSK4 (1 μg/ml) for 4 h and were transfected with 2 μg/ml E. coli O111:B4 LPS with Fugene HD. IL-1β release were measured after 16 h. ELISA supernatants were added to IL-1α, IL-1β, IL-6, IL-12, and TNF-α capture antibody-coated 96-well plates and incubated at 4°C overnight. Plates were incubated with the appropriate biotinylated antibodies in 1% BSA, followed by streptavidin. ELISA was developed with o-phenylenediamine dihydrochloride in citric acid buffer and stopped with 3M sulfuric acid. Plates were read on a spectrophotometer at 490 nm.

Hyperactivation

Triplicate wells of BMDMs were seeded in TC-treated 48 well plates (ELISA, LDH), and 12 well plates (western). All conditions except untreated were primed with 1 ug/mL LPS for 4 hrs. BMDMs were infected with *S.* Tm. (MOI 20) or *ΔoatA S. aureus* (MOI 30 or 60) as described above. Gentamycin (100 ug/mL) was added 1 hr post infection. Sups and lysates were harvested at 30 min (*S.* Tm.) or 2 and 6 hrs (*ΔoatA*) and analyzed by ELISA for IL-1B release, by LDH for cytotoxicity, or by western blotting for caspase-1, GSDMD, CARD19, and actin (loading control).

SNP Sequencing

Tails from four *Card19*$^{-/-}$ mice were sent to Dartmouse for a genetic background check. Each sample was interrogated over 5300 SNPs space along the mouse genome with an average density of 0.5 Mbp using an Illumina Infinium Genotyping Assay.

Whole Exome Sequencing
Genomic DNA was extracted from 1 B6 and two *Card19*$^{-/-}$ BMDMs derived from three independent mice using a DNeasy blood and tissue kit (Qiagen) according to the manufacturer's instructions. gDNA was shipped to Genewiz for Illumina HiSeq 2x150 bp sequencing. C57BL/6J was used as a reference genome.

RNA-seq
B6 and *Card19*$^{-/-}$ BMDMs were prepared as above from 3 independent mice per genotype. 1×10^6 BMDMs were treated with 100 ng/mL for 3 hours or left untreated. RNA was extracted using the RNeasy Plus Mini Kit (Qiagen) according to the manufacturer's instructions. Sequence-ready libraries were prepared using the Illumina TruSeq Total Transcriptome kit with Ribo-Zero Gold rRNA depletion (Illumina). Quality assessment and quantification of RNA preparations and libraries were carried out using an Agilent 4200 TapeStation and Qubit 3, respectively. Samples were sequenced on an Illumina NextSeq 500 to produce 75–base pair single end reads with a mean sequencing depth of 35 million reads per sample. Raw reads from this study were mapped to the mouse reference transcriptome (Ensembl; Mus musculus GRCm38) using Kallisto version 0.46.2 (96). Raw sequence data are available on the Gene Expression Omnibus (GEO; accession no. GSE168489)

All subsequent analyses were carried out using the statistical computing environment R version 4.0.3 in RStudio version 1.2.5042 and Bioconductor (97). Briefly, transcript quantification data were summarized to genes using the tximport package (98) and normalized using the trimmed mean of M values (TMM) method in edgeR (99). Genes with <1 CPM in 2 samples were filtered out. Normalized filtered data were variance-stabilized using the voom function in limma (100), and differentially expressed genes were identified with linear modeling using limma (FDR ≤ 0.10; absolute $\log_2$FC ≥ 1) after correcting for multiple testing using Benjamini-Hochberg. Volcano plots were made using the Enhanced Volcano package (101).

Mouse infections
Age and sex-matched B6 and *Card19*$^{-/-}$ mice between 8-12 weeks were orally infected with 10^8 CFU of *Yersinia pseudotuberculosis* strain IP2777 after fasting overnight. Mice were monitored for survival for 30 days or were euthanized using CO_2 followed by cervical dislocation, in compliance with IACUC approved euthanasia protocols. Blood was harvested by cardiac puncture following death. Serum cytokine levels (IL-6, IL-12, TNF-α) were measured by ELISAs as described above. Spleen, liver, mesenteric lymph nodes, and Peyer's patches were removed, weighed, homogenized, diluted in PBS, and plated on LB agar plates with irgasan for CFUs.

Thioglycolate Injections
Age and sex-matched B6 and *Card19*$^{-/-}$ mice between 9-11 weeks were injected intraperitoneally with 4% aged thioglycolate or PBS. 48 hours after injection, mice were euthanized using CO_2. The peritoneum was lavaged with 10 mL cold PBS and the peritoneal exudate cells were spun down. RBCs were lysed using RBC lysis buffer. PECS were counted using trypan blue exclusion on a hemocytometer and plated in complete DMEM without antibiotics in 96 well plates (1×10^5 cells for PBS PECS, 0.7×10^5 cells for TG PECS). Cells were washed with warm PBS to remove non-adherent cells and infected with *Yp*, *S.* Tm. or treated with staurosporine as described above.

Statistical Analysis
Statistical analysis was completed using GraphPad Prism. Two-tailed Student's *t* test or paired Student's *t* test were used for comparisons of two groups. One-way analysis of variance (ANOVA) with pairwise comparisons and Bonferroni post-test correction was used for multiple group comparisons. Repeated-measures ANOVA or paired *t* tests were used for matched samples. Studies were conducted without blinding or randomization. Values of $p < 0.05$ were considered statistically significant

References

1. Mori C, Nakamura N, Kimura S, Irie H, Takigawa T, Shiota K. Programmed cell death in the interdigital tissue of the fetal mouse limb is apoptosis with DNA fragmentation. Anat Rec. 1995;242(1):103-10.
2. Rodriguez I, Ody C, Araki K, Garcia I, Vassalli P. An early and massive wave of germinal cell apoptosis is required for the development of functional spermatogenesis. EMBO J. 1997;16(9):2262-70.
3. Kajstura J, Cheng W, Reiss K, Clark WA, Sonnenblick EH, Krajewski S, et al. Apoptotic and necrotic myocyte cell deaths are independent contributing variables of infarct size in rats. Lab Invest. 1996;74(1):86-107.
4. Mariathasan S, Newton K, Monack DM, Vucic D, French DM, Lee WP, et al. Differential activation of the inflammasome by caspase-1 adaptors ASC and Ipaf. Nature. 2004;430(6996):213-8.
5. Miao EA, Alpuche-Aranda CM, Dors M, Clark AE, Bader MW, Miller SI, et al. Cytoplasmic flagellin activates caspase-1 and secretion of interleukin 1beta via Ipaf. Nat Immunol. 2006;7(6):569-75.
6. Monack DM, Mecsas J, Ghori N, Falkow S. *Yersinia* signals macrophages to undergo apoptosis and YopJ is necessary for this cell death. Proc Natl Acad Sci USA. 1997;94(19):10385-90.
7. Zamboni DS, Kobayashi KS, Kohlsdorf T, Ogura Y, Long EM, Vance RE, et al. The Birc1e cytosolic pattern-recognition receptor contributes to the detection and control of Legionella pneumophila infection. Nat Immunol. 2006;7(3):318-25.
8. Green DR, Ferguson T, Zitvogel L, Kroemer G. Immunogenic and tolerogenic cell death. Nat Rev Immunol. 2009;9(5):353-63.
9. Kerr JF, Wyllie AH, Currie AR. Apoptosis: a basic biological phenomenon with wide-ranging implications in tissue kinetics. Br J Cancer. 1972;26(4):239-57.
10. Uchiyama R, Yonehara S, Taniguchi S, Ishido S, Ishii KJ, Tsutsui H. Inflammasome and Fas-Mediated IL-1beta Contributes to Th17/Th1 Cell Induction in Pathogenic Bacterial Infection In Vivo. J Immunol. 2017;199(3):1122-30.
11. Nagata S. Apoptosis and Clearance of Apoptotic Cells. Annu Rev Immunol. 2018.
12. Samali A, Zhivotovsky B, Jones D, Nagata S, Orrenius S. Apoptosis: cell death defined by caspase activation. Cell Death Differ. 1999;6(6):495-6.
13. Fink SL, Cookson BT. Apoptosis, pyroptosis, and necrosis: mechanistic description of dead and dying eukaryotic cells. Infect Immun. 2005;73(4):1907-16.
14. Kayagaki N, Stowe IB, Lee BL, O'Rourke K, Anderson K, Warming S, et al. Caspase-11 cleaves gasdermin D for non-canonical inflammasome signalling. Nature. 2015;526(7575):666-71.
15. Martinon F, Burns K, Tschopp J. The inflammasome: a molecular platform triggering activation of inflammatory caspases and processing of proIL-beta. Mol Cell. 2002;10(2):417-26.
16. Shi J, Zhao Y, Wang K, Shi X, Wang Y, Huang H, et al. Cleavage of GSDMD by inflammatory caspases determines pyroptotic cell death. Nature. 2015;526(7575):660-5.
17. Orning P, Weng D, Starheim K, Ratner D, Best Z, Lee B, et al. Pathogen blockade of TAK1 triggers caspase-8–dependent cleavage of gasdermin D and cell death. Science. 2018:eaau2818.
18. Sarhan J, Liu BC, Muendlein HI, Li P, Nilson R, Tang AY, et al. Caspase-8 induces cleavage of gasdermin D to elicit pyroptosis during Yersinia infection. Proc Natl Acad Sci U S A. 2018;115(46):E10888-E97.
19. Chen KW, Demarco B, Heilig R, Shkarina K, Boettcher A, Farady CJ, et al. Extrinsic and intrinsic apoptosis activate pannexin-1 to drive NLRP3 inflammasome assembly. Embo j. 2019;38(10).
20. Demarco B, Grayczyk JP, Bjanes E, Le Roy D, Tonnus W, Assenmacher CA, et al. Caspase-8-dependent gasdermin D cleavage promotes antimicrobial defense but confers susceptibility to TNF-induced lethality. Science advances. 2020;6(47).
21. Demarco B, Chen KW, Broz P. Cross talk between intracellular pathogens and cell death. Immunol Rev. 2020;297(1):174-93.
22. Cullen SP, Kearney CJ, Clancy DM, Martin SJ. Diverse Activators of the NLRP3 Inflammasome Promote IL-1beta Secretion by Triggering Necrosis. Cell Rep. 2015;11(10):1535-48.

23. Kayagaki N, Warming S, Lamkanfi M, Vande Walle L, Louie S, Dong J, et al. Non-canonical inflammasome activation targets caspase-11. Nature. 2011;479(7371):117-21.
24. Fink SL, Cookson BT. Caspase-1-dependent pore formation during pyroptosis leads to osmotic lysis of infected host macrophages. Cell Microbiol. 2006;8(11):1812-25.
25. Verhoef PA, Kertesy SB, Lundberg K, Kahlenberg JM, Dubyak GR. Inhibitory effects of chloride on the activation of caspase-1, IL-1beta secretion, and cytolysis by the P2X7 receptor. J Immunol. 2005;175(11):7623-34.
26. Evavold CL, Ruan J, Tan Y, Xia S, Wu H, Kagan JC. The Pore-Forming Protein Gasdermin D Regulates Interleukin-1 Secretion from Living Macrophages. Immunity. 2018;48(1):35-44 e6.
27. Heilig R, Dilucca M, Boucher D, Chen KW, Hancz D, Demarco B, et al. Caspase-1 cleaves Bid to release mitochondrial SMAC and drive secondary necrosis in the absence of GSDMD. Life Science Alliance. 2020;3(6):e202000735.
28. Gaidt MM, Ebert TS, Chauhan D, Schmidt T, Schmid-Burgk JL, Rapino F, et al. Human Monocytes Engage an Alternative Inflammasome Pathway. Immunity. 2016;44(4):833-46.
29. Chen KW, Gross CJ, Sotomayor FV, Stacey KJ, Tschopp J, Sweet MJ, et al. The neutrophil NLRC4 inflammasome selectively promotes IL-1beta maturation without pyroptosis during acute Salmonella challenge. Cell Rep. 2014;8(2):570-82.
30. Zanoni I, Tan Y, Di Gioia M, Springstead JR, Kagan JC. By Capturing Inflammatory Lipids Released from Dying Cells, the Receptor CD14 Induces Inflammasome-Dependent Phagocyte Hyperactivation. Immunity. 2017;47(4):697-709.e3.
31. Zanoni I, Tan Y, Di Gioia M, Broggi A, Ruan J, Shi J, et al. An endogenous caspase-11 ligand elicits interleukin-1 release from living dendritic cells. Science. 2016;352(6290):1232-6.
32. Heilig R, Dick MS, Sborgi L, Meunier E, Hiller S, Broz P. The Gasdermin-D pore acts as a conduit for IL-1beta secretion in mice. Eur J Immunol. 2017.
33. Rios KE, Kashyap AK, Maynard SK, Washington M, Paul S, Schaefer BC. CARD19, the protein formerly known as BinCARD, is a mitochondrial protein that does not regulate Bcl10-dependent NF-κB activation after TCR engagement. Cellular Immunology. 2020;356:104179.
34. Woo HN, Hong GS, Jun JI, Cho DH, Choi HW, Lee HJ, et al. Inhibition of Bcl10-mediated activation of NF-kappa B by BinCARD, a Bcl10-interacting CARD protein. FEBS Lett. 2004;578(3):239-44.
35. Subramanian N, Natarajan K, Clatworthy MR, Wang Z, Germain RN. The adaptor MAVS promotes NLRP3 mitochondrial localization and inflammasome activation. Cell. 2013;153(2):348-61.
36. Zhou R, Yazdi AS, Menu P, Tschopp J. A role for mitochondria in NLRP3 inflammasome activation. Nature. 2011;469(7329):221-5.
37. Mills EL, Kelly B, O'Neill LAJ. Mitochondria are the powerhouses of immunity. Nat Immunol. 2017;18(5):488-98.
38. Seth RB, Sun L, Ea C-K, Chen ZJ. Identification and Characterization of MAVS, a Mitochondrial Antiviral Signaling Protein that Activates NF-κB and IRF3. Cell. 2005;122(5):669-82.
39. Elliott EI, Miller AN, Banoth B, Iyer SS, Stotland A, Weiss JP, et al. Cutting Edge: Mitochondrial Assembly of the NLRP3 Inflammasome Complex Is Initiated at Priming. The Journal of Immunology. 2018:ji1701723.
40. Kayagaki N, Kornfeld OS, Lee BL, Stowe IB, O'Rourke K, Li Q, et al. NINJ1 mediates plasma membrane rupture during lytic cell death. Nature. 2021.
41. Carty M, Kearney J, Shanahan KA, Hams E, Sugisawa R, Connolly D, et al. Cell Survival and Cytokine Release after Inflammasome Activation Is Regulated by the Toll-IL-1R Protein SARM. Immunity. 2019;50(6):1412-24.e6.
42. Lissner CR, Weinstein DL, O'Brien AD. Mouse chromosome 1 Ity locus regulates microbicidal activity of isolated peritoneal macrophages against a diverse group of intracellular and extracellular bacteria. J Immunol. 1985;135(1):544-7.
43. Stach JL, Gros P, Forget A, Skamene E. Phenotypic expression of genetically-controlled natural resistance to Mycobacterium bovis (BCG). J Immunol. 1984;132(2):888-92.

44. Roberts JE, Watters JW, Ballard JD, Dietrich WF. Ltx1, a mouse locus that influences the susceptibility of macrophages to cytolysis caused by intoxication with Bacillus anthracis lethal factor, maps to chromosome 11. Mol Microbiol. 1998;29(2):581-91.
45. Watson J, Kelly K, Largen M, Taylor BA. The genetic mapping of a defective LPS response gene in C3H/HeJ mice. J Immunol. 1978;120(2):422-4.
46. Franchi L, Amer A, Body-Malapel M, Kanneganti TD, Ozoren N, Jagirdar R, et al. Cytosolic flagellin requires Ipaf for activation of caspase-1 and interleukin 1beta in *Salmonella*-infected macrophages. Nat Immunol. 2006;7(6):576-82.
47. Kofoed EM, Vance RE. Innate immune recognition of bacterial ligands by NAIPs determines inflammasome specificity. Nature. 2011;477(7366):592-5.
48. Mariathasan S, Weiss DS, Newton K, McBride J, O'Rourke K, Roose-Girma M, et al. Cryopyrin activates the inflammasome in response to toxins and ATP. Nature. 2006;440(7081):228-32.
49. Munoz-Planillo R, Kuffa P, Martinez-Colon G, Smith BL, Rajendiran TM, Nunez G. K(+) efflux is the common trigger of NLRP3 inflammasome activation by bacterial toxins and particulate matter. Immunity. 2013;38(6):1142-53.
50. Perregaux D, Gabel CA. Interleukin-1 beta maturation and release in response to ATP and nigericin. Evidence that potassium depletion mediated by these agents is a necessary and common feature of their activity. J Biol Chem. 1994;269(21):15195-203.
51. Solle M, Labasi J, Perregaux DG, Stam E, Petrushova N, Koller BH, et al. Altered cytokine production in mice lacking P2X(7) receptors. J Biol Chem. 2001;276(1):125-32.
52. Sutterwala FS, Ogura Y, Szczepanik M, Lara-Tejero M, Lichtenberger GS, Grant EP, et al. Critical role for NALP3/CIAS1/Cryopyrin in innate and adaptive immunity through its regulation of caspase-1. Immunity. 2006;24(3):317-27.
53. Philip NH, Dillon CP, Snyder AG, Fitzgerald P, Wynosky-Dolfi MA, Zwack EE, et al. Caspase-8 mediates caspase-1 processing and innate immune defense in response to bacterial blockade of NF-kappaB and MAPK signaling. Proc Natl Acad Sci U S A. 2014;111(20):7385-90.
54. Zhang Y, Ting AT, Marcu KB, Bliska JB. Inhibition of MAPK and NF-kappa B pathways is necessary for rapid apoptosis in macrophages infected with *Yersinia*. J Immunol. 2005;174(12):7939-49.
55. Antonopoulos C, El Sanadi C, Kaiser WJ, Mocarski ES, Dubyak GR. Proapoptotic chemotherapeutic drugs induce noncanonical processing and release of IL-1beta via caspase-8 in dendritic cells. J Immunol. 2013;191(9):4789-803.
56. Bertrand R, Solary E, O'Connor P, Kohn KW, Pommier Y. Induction of a common pathway of apoptosis by staurosporine. Exp Cell Res. 1994;211(2):314-21.
57. Jacobsen MD, Weil M, Raff MC. Role of Ced-3/ICE-family proteases in staurosporine-induced programmed cell death. J Cell Biol. 1996;133(5):1041-51.
58. Degterev A, Hitomi J, Germscheid M, Ch'en IL, Korkina O, Teng X, et al. Identification of RIP1 kinase as a specific cellular target of necrostatins. Nat Chem Biol. 2008;4(5):313-21.
59. He S, Liang Y, Shao F, Wang X. Toll-like receptors activate programmed necrosis in macrophages through a receptor-interacting kinase-3-mediated pathway. Proc Natl Acad Sci U S A. 2011;108(50):20054-9.
60. Ghosn EEB, Cassado AA, Govoni GR, Fukuhara T, Yang Y, Monack DM, et al. Two physically, functionally, and developmentally distinct peritoneal macrophage subsets. Proceedings of the National Academy of Sciences. 2010;107(6):2568.
61. Okabe Y, Medzhitov R. Tissue-specific signals control reversible program of localization and functional polarization of macrophages. Cell. 2014;157(4):832-44.
62. Bell CW, Jiang W, Reich CF, 3rd, Pisetsky DS. The extracellular release of HMGB1 during apoptotic cell death. Am J Physiol Cell Physiol. 2006;291(6):C1318-25.
63. Broz P, Dixit VM. Inflammasomes: mechanism of assembly, regulation and signalling. Nat Rev Immunol. 2016;16(7):407-20.
64. Martinon F, Gaide O, Petrilli V, Mayor A, Tschopp J. NALP inflammasomes: a central role in innate immunity. Seminars in immunopathology. 2007;29(3):213-29.
65. Aglietti RA, Estevez A, Gupta A, Ramirez MG, Liu PS, Kayagaki N, et al. GsdmD p30 elicited by caspase-11 during pyroptosis forms pores in membranes. Proc Natl Acad Sci U S A. 2016;113(28):7858-63.

66. Liu X, Zhang Z, Ruan J, Pan Y, Magupalli VG, Wu H, et al. Inflammasome-activated gasdermin D causes pyroptosis by forming membrane pores. Nature. 2016;535(7610):153-8.
67. Kischkel FC, Hellbardt S, Behrmann I, Germer M, Pawlita M, Krammer PH, et al. Cytotoxicity-dependent APO-1 (Fas/CD95)-associated proteins form a death-inducing signaling complex (DISC) with the receptor. EMBO J. 1995;14(22):5579-88.
68. Wallach D, Boldin M, Varfolomeev E, Beyaert R, Vandenabeele P, Fiers W. Cell death induction by receptors of the TNF family: towards a molecular understanding. FEBS letters. 1997;410(1):96-106.
69. Denecker G, Declercq W, Geuijen CA, Boland A, Benabdillah R, van Gurp M, et al. *Yersinia enterocolitica* YopP-induced apoptosis of macrophages involves the apoptotic signaling cascade upstream of bid. J Biol Chem. 2001;276(23):19706-14.
70. Li H, Zhu H, Xu CJ, Yuan J. Cleavage of BID by caspase 8 mediates the mitochondrial damage in the Fas pathway of apoptosis. Cell. 1998;94(4):491-501.
71. Rogers C, Fernandes-Alnemri T, Mayes L, Alnemri D, Cingolani G, Alnemri ES. Cleavage of DFNA5 by caspase-3 during apoptosis mediates progression to secondary necrotic/pyroptotic cell death. Nat Commun. 2017;8:14128.
72. Bossaller L, Chiang PI, Schmidt-Lauber C, Ganesan S, Kaiser WJ, Rathinam VA, et al. Cutting edge: FAS (CD95) mediates noncanonical IL-1beta and IL-18 maturation via caspase-8 in an RIP3-independent manner. J Immunol. 2012;189(12):5508-12.
73. Conos SA, Lawlor KE, Vaux DL, Vince JE, Lindqvist LM. Cell death is not essential for caspase-1-mediated interleukin-1beta activation and secretion. Cell Death Differ. 2016;23(11):1827-38.
74. Zwack EE, Feeley EM, Burton AR, Hu B, Yamamoto M, Kanneganti TD, et al. Guanylate Binding Proteins Regulate Inflammasome Activation in Response to Hyperinjected Yersinia Translocon Components. Infect Immun. 2017;85(10).
75. Zwack EE, Snyder AG, Wynosky-Dolfi MA, Ruthel G, Philip NH, Marketon MM, et al. Inflammasome activation in response to the Yersinia type III secretion system requires hyperinjection of translocon proteins YopB and YopD. MBio. 2015;6(1):e02095-14.
76. Wolf AJ, Reyes CN, Liang W, Becker C, Shimada K, Wheeler ML, et al. Hexokinase Is an Innate Immune Receptor for the Detection of Bacterial Peptidoglycan. Cell. 2016;166(3):624-36.
77. Peterson LW, Philip NH, DeLaney A, Wynosky-Dolfi MA, Asklof K, Gray F, et al. RIPK1-dependent apoptosis bypasses pathogen blockade of innate signaling to promote immune defense. J Exp Med. 2017;214(11):3171-82.
78. Weng D, Marty-Roix R, Ganesan S, Proulx MK, Vladimer GI, Kaiser WJ, et al. Caspase-8 and RIP kinases regulate bacteria-induced innate immune responses and cell death. Proceedings of the National Academy of Sciences of the United States of America. 2014;111(20):7391-6.
79. Peterson LW, Philip NH, Dillon CP, Bertin J, Gough PJ, Green DR, et al. Cell-Extrinsic TNF Collaborates with TRIF Signaling To Promote Yersinia-Induced Apoptosis. J Immunol. 2016;197(10):4110-7.
80. Wang Y, Shi P, Chen Q, Huang Z, Zou D, Zhang J, et al. Mitochondrial ROS promote macrophage pyroptosis by inducing GSDMD oxidation. Journal of Molecular Cell Biology. 2019;11(12):1069-82.
81. Kim Y, Zhou P, Qian L, Chuang J-Z, Lee J, Li C, et al. MyD88-5 links mitochondria, microtubules, and JNK3 in neurons and regulates neuronal survival. J Exp Med. 2007;204(9):2063-74.
82. Uccellini MB, Bardina SV, Sánchez-Aparicio MT, White KM, Hou Y-J, Lim JK, et al. Passenger Mutations Confound Phenotypes of SARM1-Deficient Mice. Cell Rep. 2020;31(1):107498.
83. Wang GG, Calvo KR, Pasillas MP, Sykes DB, Häcker H, Kamps MP. Quantitative production of macrophages or neutrophils ex vivo using conditional Hoxb8. Nature Methods. 2006;3(4):287-93.
84. Purtha WE, Swiecki M, Colonna M, Diamond MS, Bhattacharya D. Spontaneous mutation of the Dock2 gene in Irf5^{−/−} mice complicates interpretation of type I interferon production and antibody responses. Proceedings of the National Academy of Sciences. 2012:201118155.
85. Mahajan Vinay S, Demissie E, Mattoo H, Viswanadham V, Varki A, Morris R, et al. Striking Immune Phenotypes in Gene-Targeted Mice Are Driven by a Copy-Number Variant Originating from a Commercially Available C57BL/6 Strain. Cell Rep. 2016;15(9):1901-9.

86. Netea MG, Nold-Petry CA, Nold MF, Joosten LA, Opitz B, van der Meer JH, et al. Differential requirement for the activation of the inflammasome for processing and release of IL-1beta in monocytes and macrophages. Blood. 2009;113(10):2324-35.
87. Evavold CL, Hafner-Bratkovič I, Kagan JC. Downstream of gasdermin D cleavage, a Ragulator-Rag-mTORC1 pathway promotes pore formation and pyroptosis. bioRxiv. 2020:2020.11.02.362517.
88. Rogers C, Erkes DA, Nardone A, Aplin AE, Fernandes-Alnemri T, Alnemri ES. Gasdermin pores permeabilize mitochondria to augment caspase-3 activation during apoptosis and inflammasome activation. Nature Communications. 2019;10(1):1689.
89. Diez E, Lee SH, Gauthier S, Yaraghi Z, Tremblay M, Vidal S, et al. Birc1e is the gene within the Lgn1 locus associated with resistance to Legionella pneumophila. Nat Genet. 2003;33(1):55-60.
90. Brodsky IE, Palm NW, Sadanand S, Ryndak MB, Sutterwala FS, Flavell RA, et al. A Yersinia effector protein promotes virulence by preventing inflammasome recognition of the type III secretion system. Cell Host Microbe. 2010;7(5):376-87.
91. Szretter KJ, Daffis S, Patel J, Suthar MS, Klein RS, Gale M, Jr., et al. The innate immune adaptor molecule MyD88 restricts West Nile virus replication and spread in neurons of the central nervous system. J Virol. 2010;84(23):12125-38.
92. Rauch I, Deets KA, Ji DX, von Moltke J, Tenthorey JL, Lee AY, et al. NAIP-NLRC4 Inflammasomes Coordinate Intestinal Epithelial Cell Expulsion with Eicosanoid and IL-18 Release via Activation of Caspase-1 and -8. Immunity. 2017;46(4):649-59.
93. Newton K, Sun X, Dixit VM. Kinase RIP3 is dispensable for normal NF-kappa Bs, signaling by the B-cell and T-cell receptors, tumor necrosis factor receptor 1, and Toll-like receptors 2 and 4. Mol Cell Biol. 2004;24(4):1464-9.
94. Oberst A, Dillon CP, Weinlich R, McCormick LL, Fitzgerald P, Pop C, et al. Catalytic activity of the caspase-8-FLIP(L) complex inhibits RIPK3-dependent necrosis. Nature. 2011;471(7338):363-7.
95. Wang S, Miura M, Jung YK, Zhu H, Li E, Yuan J. Murine caspase-11, an ICE-interacting protease, is essential for the activation of ICE. Cell. 1998;92(4):501-9.
96. Bray NL, Pimentel H, Melsted P, Pachter L. Near-optimal probabilistic RNA-seq quantification. Nat Biotechnol. 2016;34(5):525-7.
97. Huber W, Carey VJ, Gentleman R, Anders S, Carlson M, Carvalho BS, et al. Orchestrating high-throughput genomic analysis with Bioconductor. Nature Methods. 2015;12(2):115-21.
98. Soneson C, Love MI, Robinson MD. Differential analyses for RNA-seq: transcript-level estimates improve gene-level inferences. F1000Research. 2015;4:1521.
99. Robinson MD, McCarthy DJ, Smyth GK. edgeR: a Bioconductor package for differential expression analysis of digital gene expression data. Bioinformatics. 2010;26(1):139-40.
100. Ritchie ME, Phipson B, Wu D, Hu Y, Law CW, Shi W, et al. limma powers differential expression analyses for RNA-sequencing and microarray studies. Nucleic Acids Res. 2015;43(7):e47.
101. EnhancedVolcano: Publication-ready volcano plots with enhanced colouring and labeling. [Internet]. 2018. Available from: https://github.com/kevinblighe/EnhancedVolcano.

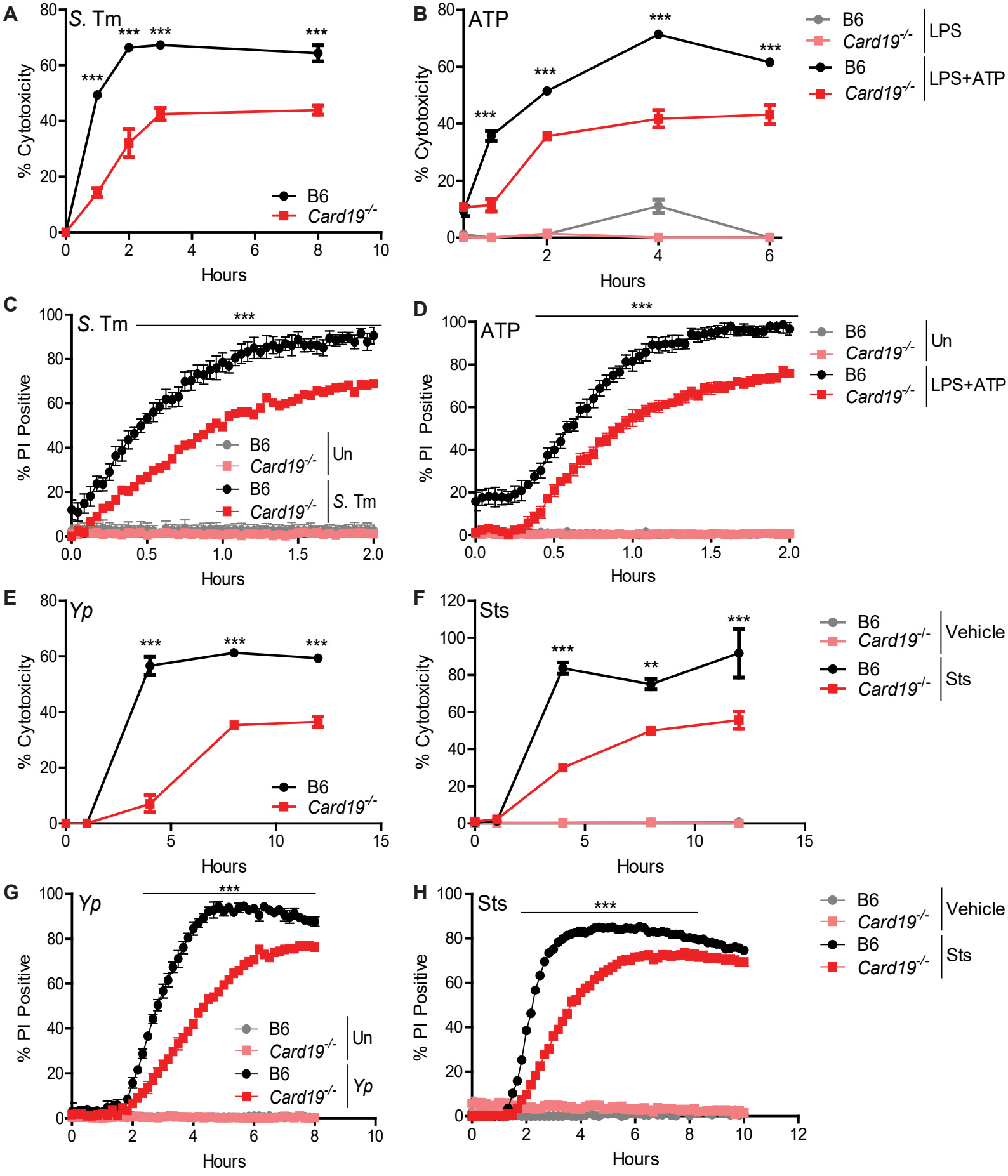

Fig. 1. *Card19*$^{-/-}$ BMDMs are deficient for caspase-dependent cell death

Primary C57BL/6J (B6) or *Card19*$^{-/-}$ BMDMs were infected with *Salmonella* Typhimurium (*S*. Tm) or *Y. pseudotuberculosis* (*Yp*), or treated with LPS+ATP or staurosporine (Sts), as indicated, and the kinetics of cell death was assayed by release of lactate dehydrogenase (LDH) (A, B, E, F) or propidium iodide (PI) uptake (C, D, G, H). Each figure is representative of three or more independent experiments. LDH release was assayed at specific times post-infection. PI uptake was measured over a two or ten-hour timecourse with fluorometric measurements taken at 2.5 minute (C, D) or 10 minute (G, H) intervals. Mean ± SEM of triplicate wells is displayed. Each panel is representative of three or more independent experiments. *** $p < 0.001$, ** $p < 0.01$, * $p < 0.05$. n.s. not significant, analyzed by 2-way ANOVA with Bonferroni multiple comparisons post-test.

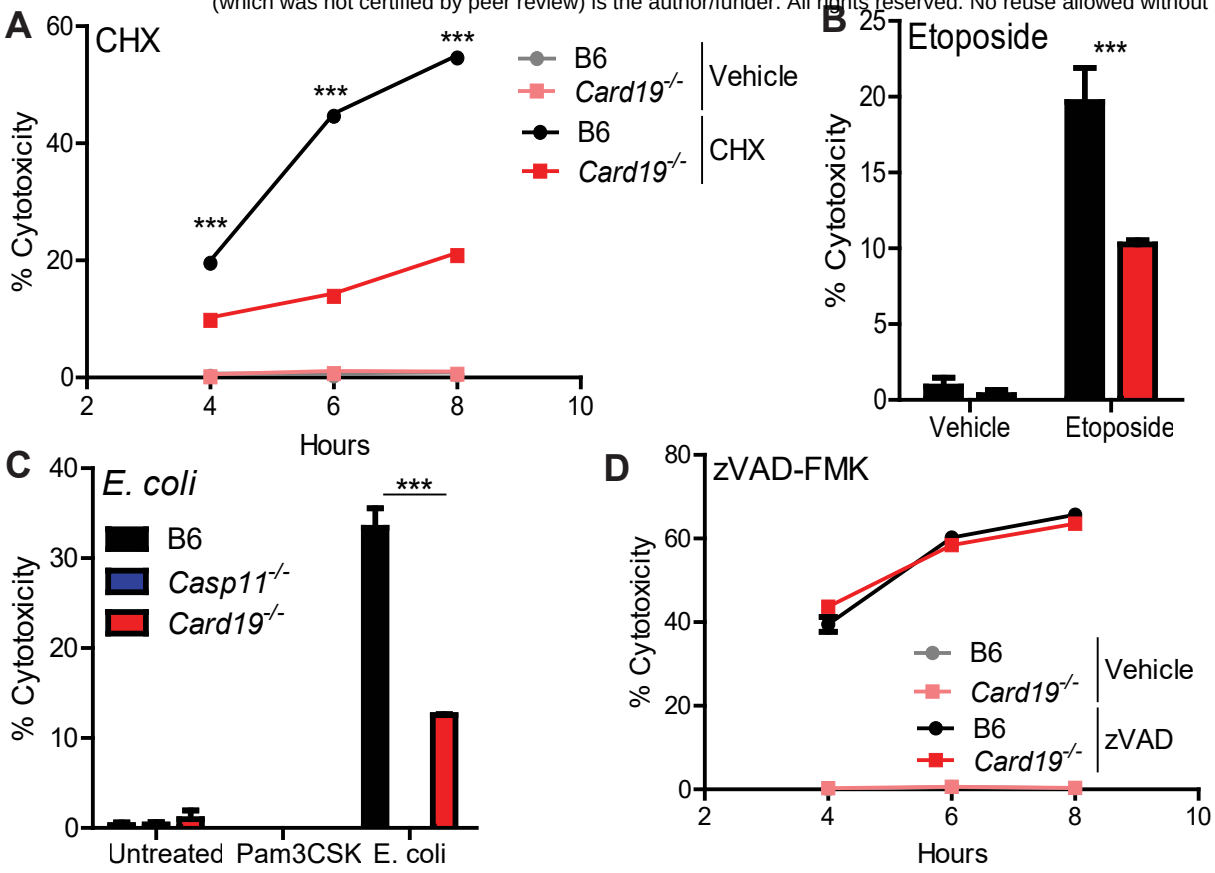

Fig. 2. *Card19*$^{-/-}$ BMDMs are caspase-dependent cell death but not necroptosis

Primary C57BL/6J (B6), *Card19*$^{-/-}$, *Card19*$^{+/+}$, and *Casp11*$^{-/-}$ BMDMs were treated with (A) Cycloheximide (CHX) (B) etoposide, (C) Pam3CSK+*E. coli* or (D) z-VAD-FMK + LPS and cell death was assayed by LDH release. BMDMs were treated, supernatants were harvested from triplicate wells at indicated time points and measured for cytotoxicity. Mean ± SEM of triplicate wells is displayed. Each figure is representative of 2 or more independent experiments. *** $p < 0.001$, ** $p < 0.01$, * $p < 0.05$. n.s. not significant. 2-way ANOVA with Bonferroni multiple comparisons post-test.

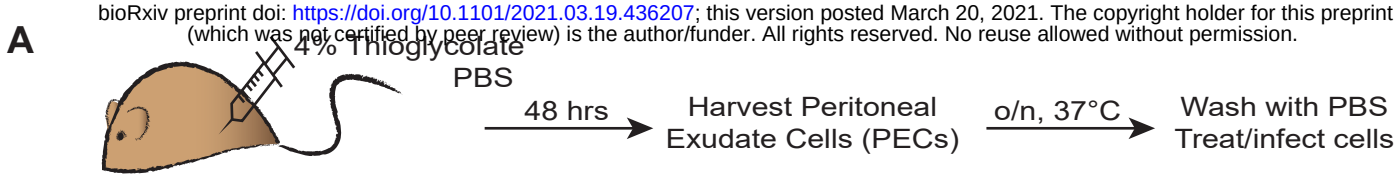

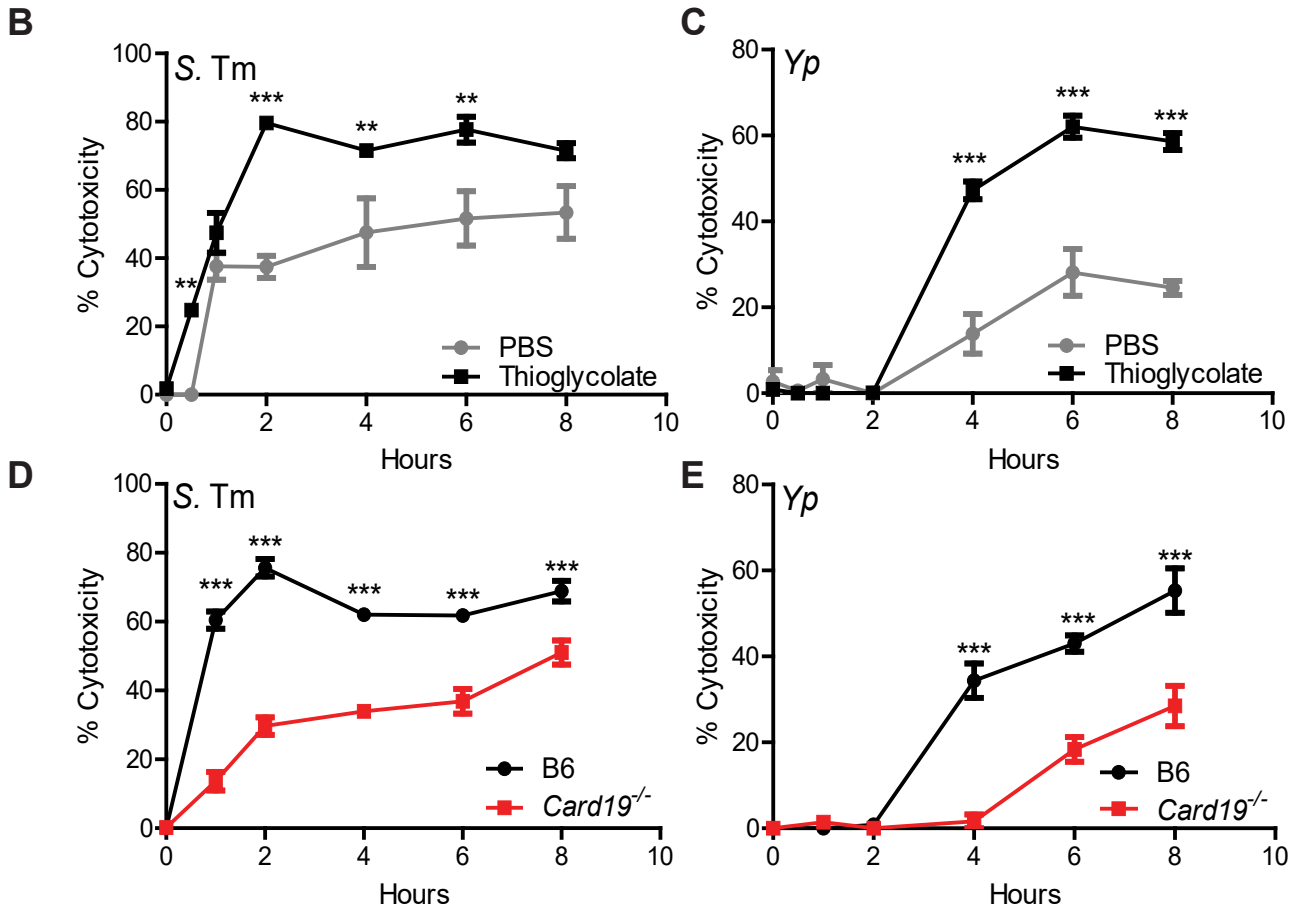

Fig. 3. Peritoneal macrophages from *Card19*$^{-/-}$ mice have reduced levels of cell death

(A) B6 and *Card19*$^{-/-}$ mice were injected with 4% aged thioglycolate or PBS. 48 hrs later, PECS were harvested, RBC lysed, counted and plated in triplicate overnight at 37°C. PBS PECS were pooled prior to plating. Cells were washed with PBS to remove non-adherent cells and infected with *Yp* or *S.* Tm (MOI 10) or treated with staurosporine (10 uM). Cytotoxicity was measured by LDH release at indicated time points. *** $p < 0.001$, ** $p < 0.01$, * $p < 0.05$. n.s. not significant. 2-way ANOVA with Bonferroni multiple comparisons post-test. Graphs are representative of two independent experiments with 3-6 mice per group, per genotype.

(B, C) PBS: mean ± SEM for technical replicates of 3 pooled B6 mice. Thioglycolate: means of technical replicates for 3 B6 mice ± SEM. Cells were infected with (B) *S.* Tm or (C) *Yp*.

(D, E) PBS: mean ± SEM for technical replicates of 4-6 pooled B6 and *Card19*$^{-/-}$ mice + SEM. Thioglycolate: means of technical replicates for 4 B6 and *Card19*$^{-/-}$ mice ± SEM. Cells were infected with (B) *S.* Tm or (C) *Yp*.

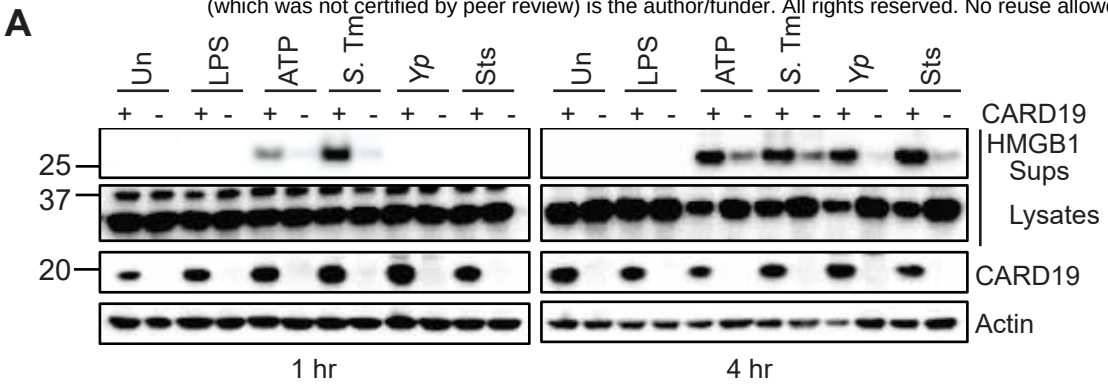

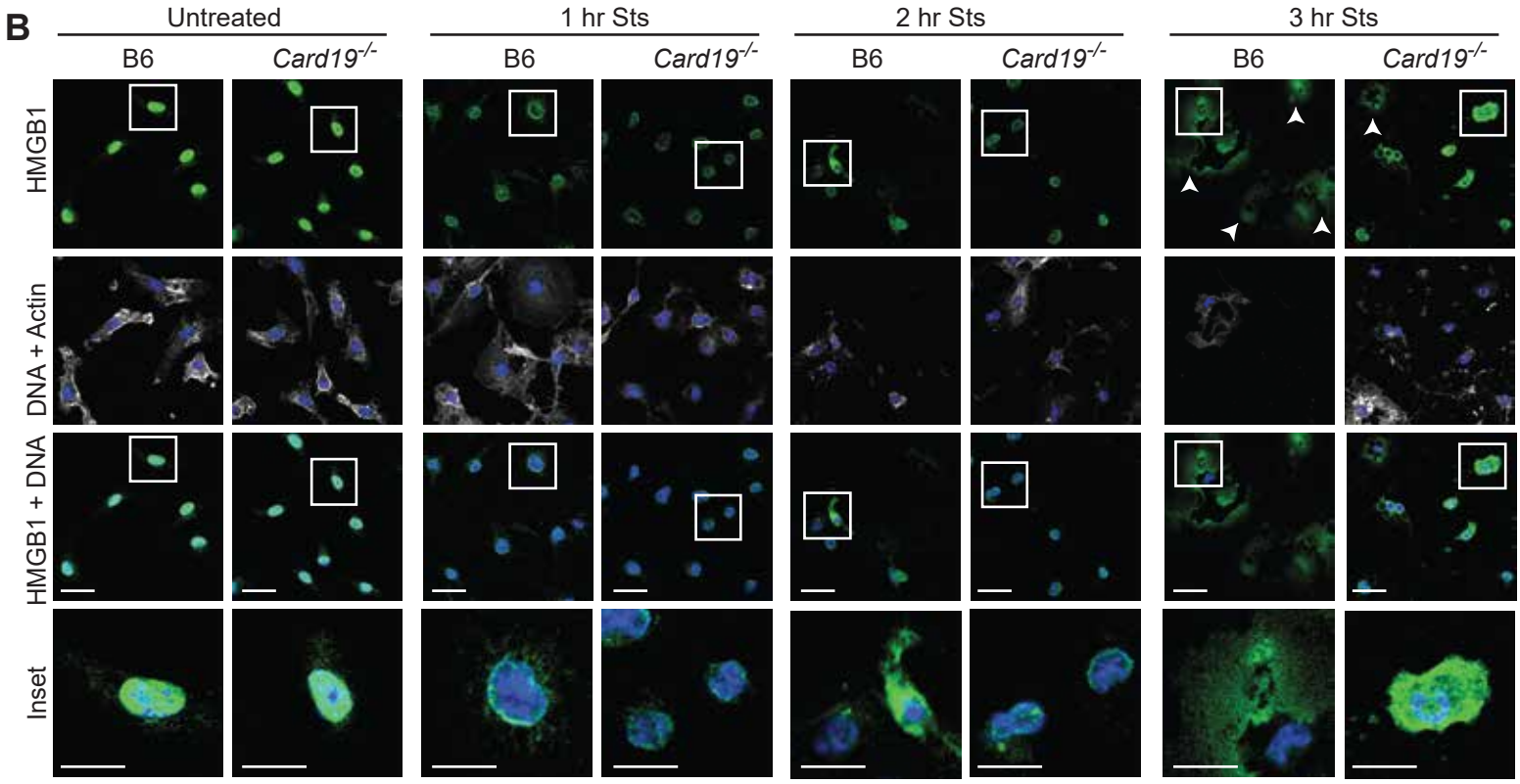

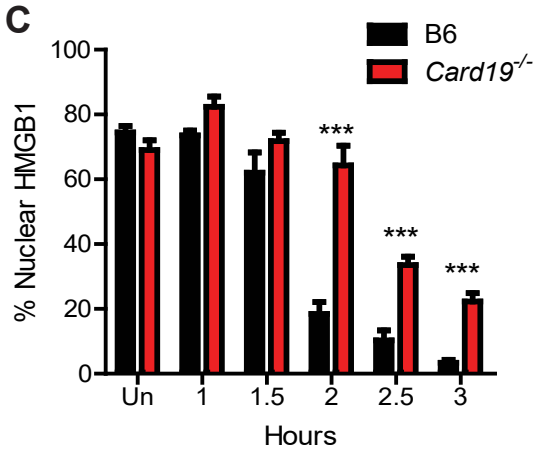

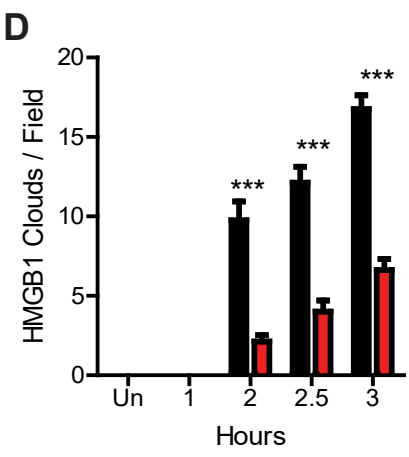

Fig. 4. *Card19*$^{-/-}$ BMDMs retain intracellular alarmin HMGB1 following activation of cell death

(A) Primary BMDMs from B6 (+) or *Card19*$^{-/-}$ (-) mice were treated with indicated treatments or infections, and TCA precipitated supernatants (Sups) or whole cell lysates (Lysates) were harvested at 1 or 4 hours post-infection and analyzed by western blotting for HMGB1, CARD19, and actin (loading control). ATP indicates cells that were primed with LPS for 3 hours and treated with ATP for 1 or 4 hours. *S.Tm* – *Salmonella* Typhimurium; *Yp Yersinia pseudotuberculosis.* Sts – staurosporine.

(B) Confocal microscopy images of untreated and staurosporine- (Sts) treated B6 and *Card19*$^{-/-}$ BMDMs fixed at indicated times post-Sts treatment and stained for HMGB1, Actin and DNA (Hoescht). White arrows indicate HMGB1 clouds. Scale bar 20 microns, inset 10 microns.

(C) Quantification of nuclear HMGB1. n=25-50 cells per field, 5-8 fields per condition, per timepoint.

(D) Quantification of HMGB1 clouds in B6 and *Card19*$^{-/-}$ BMDMs after staurosporine treatment. 5-8 fields quantified per condition, per timepoint. Mean ± SEM is displayed. *** $p < 0.001$, ** $p < 0.01$, * $p < 0.05$. n.s. not significant. 2-way ANOVA with Bonferroni multiple comparisons post-test. Representative of 3 (A-C) or 2 (D) independent experiments.

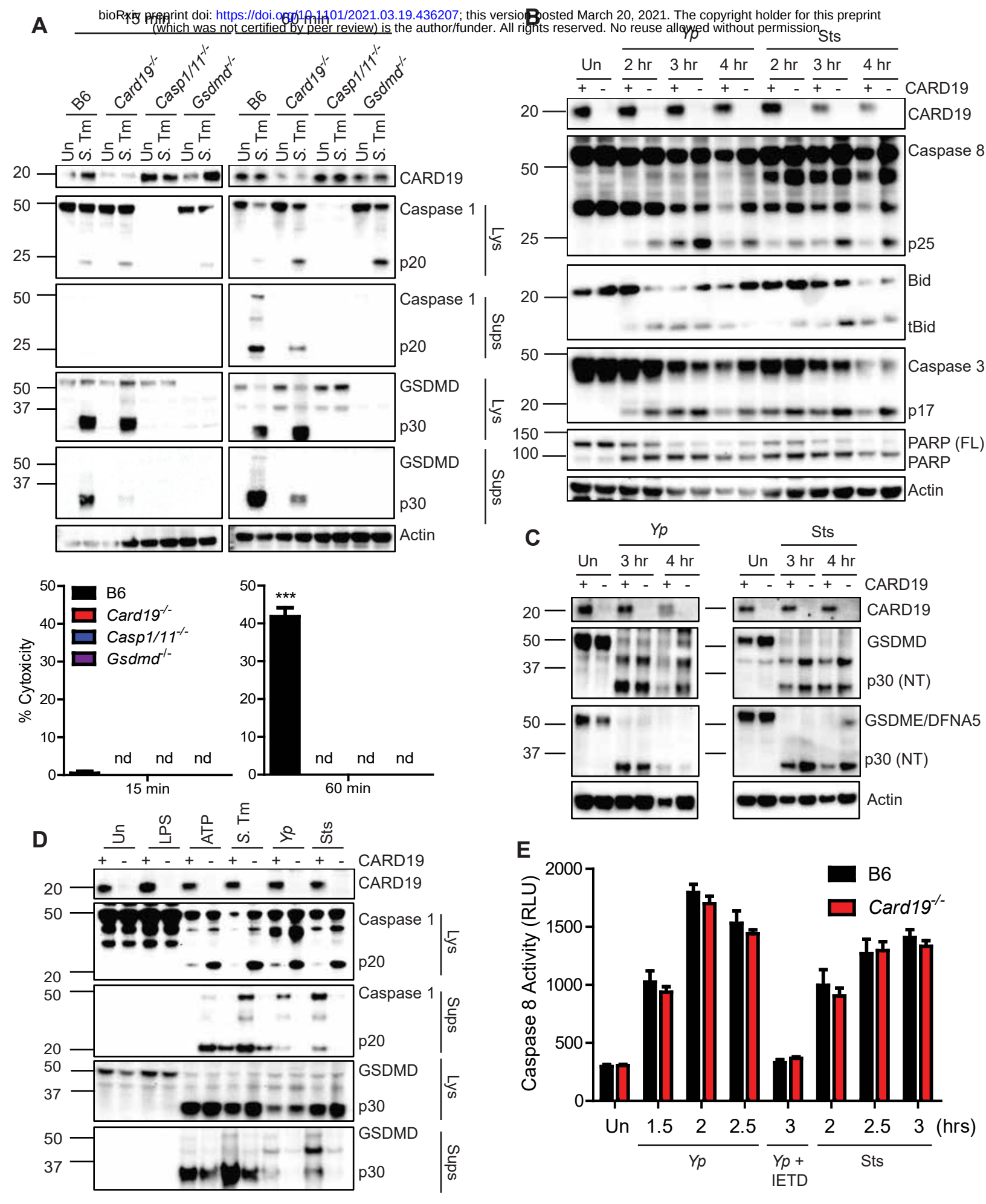

5

Fig. 5. *Card19*$^{-/-}$ macrophages are not deficient in activation of caspase-1 or -8

(A) B6, *Card19*$^{-/-}$, *Casp1/11*$^{-/-}$- or *Gsdmd*$^{-/-}$ BMDMs were left untreated or infected with *S*. Tm, and cell lysates (Lys) and TCA-precipitated supernatants (Sups) were run on SDS-PAGE and analyzed by western blotting for cleaved Casp1, GSDMD, or Actin (cell lysate loading control). Cell death from these cells was assayed in parallel by LDH release (indicated below blots). Mean ± SEM is displayed. 2-way ANOVA with Bonferroni multiple comparisons post-test. *** $p < 0.001$, ** $p < 0.01$, * $p < 0.05$. n.d. not detectable.

(B) B6 (+) or *Card19*$^{-/-}$ (-) BMDMs were infected with *Yp* or treated with Sts or 2, 3, or 4 hours, or left untreated (Un) as indicated. Cell lysates were prepared at indicated times and analyzed for presence of CARD19, cleaved caspase-8, tBid, cleaved caspase-3, cleaved PARP, and Actin (loading control).

(C) B6 and *Card19*$^{-/-}$ BMDMs were left untreated, infected with *Yp* or treated with staurosporine. Lysates were harvested at the indicated time points, run on SDS-PAGE and analyzed by western blotting for CARD19, GSDMD, GSDME/DFNA5, and actin (loading control).

(D) B6 (+) and *Card19*$^{-/-}$ (-) BMDMs were left untreated, treated with LPS, LPS+ATP, Sts, or infected with *S.* Tm or *Yp*. Cell lysates (Lys) and supernatants (Sups) were harvested 1 hour post-ATP or S.Tm infection or 3 hours post Sts treatment and *Yp* infection and assayed for CARD19, Caspase-1, and presence of cleaved GSDMD.

(E) B6 and *Card19*$^{-/-}$ BMDMs were left untreated, infected with *Yp*, or treated with staurosporine. BMDMs were pretreated with the caspase-8 inhibitor IETD for one hour prior to infection. Caspase-8 activity was assessed by Caspase-8-Glo. Mean ± SEM is displayed. Blots, caspase-8 activity and LDH are representative of at least 3 independent experiments.

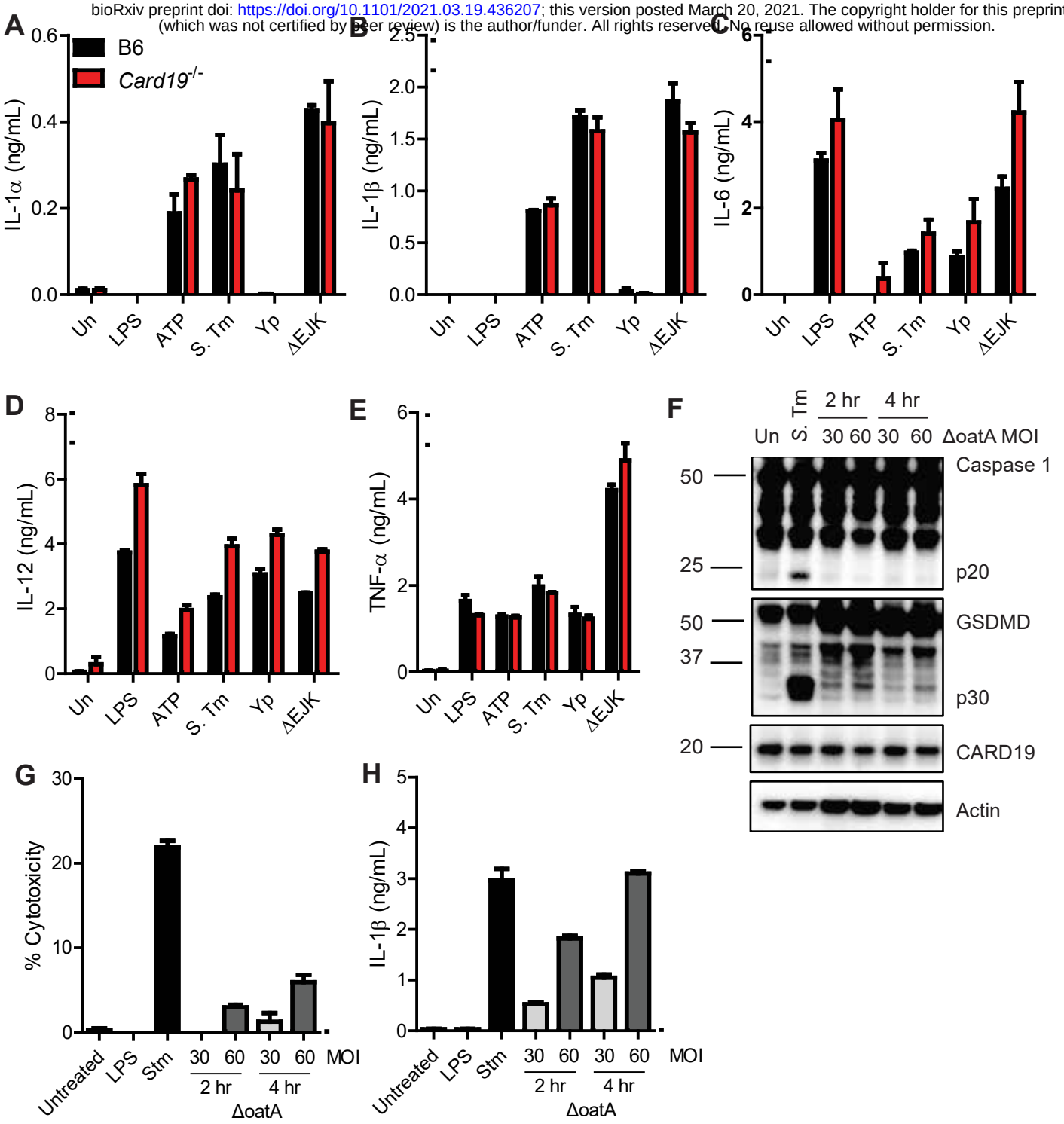

Fig. 6. The cell death defect in *Card19*$^{-/-}$ BMDMs is independent from cytokine release.

(A-E) B6 (black bars) and *Card19*$^{-/-}$ (red bars) BMDMs were primed with LPS for 3 hours and treated with extracellular ATP, infected with *S*. Tm, *Yp*, or the *Yp* ΔEJK strain lacking effectors YopE, YopJ and YopK. Supernatants were harvested 2 hours post-infection or ATP treatment and analyzed by ELISA for release of (A) IL-1α, (B) IL-1B, (C) IL-6, (D) IL-12, and (E) TNF-α. Mean ± SEM is displayed. Each figure is representative of 3 or more independent experiments.

(F-H) B6 BMDMs were primed with LPS for 4 hours and infected with Δ*oatA S. aureus* or *S.* Tm. (F) Lysates were harvested at indicated times, run on SDS-PAGE page and analyzed by western blotting for Caspase 1, GSDMD, CARD19, or Actin (loading control). Supernatants were harvested at indicated time points and analyzed by (G) LDH for cytotoxicity and (H) ELISA for release of IL-1β. Each figure is representative of two independent experiments.

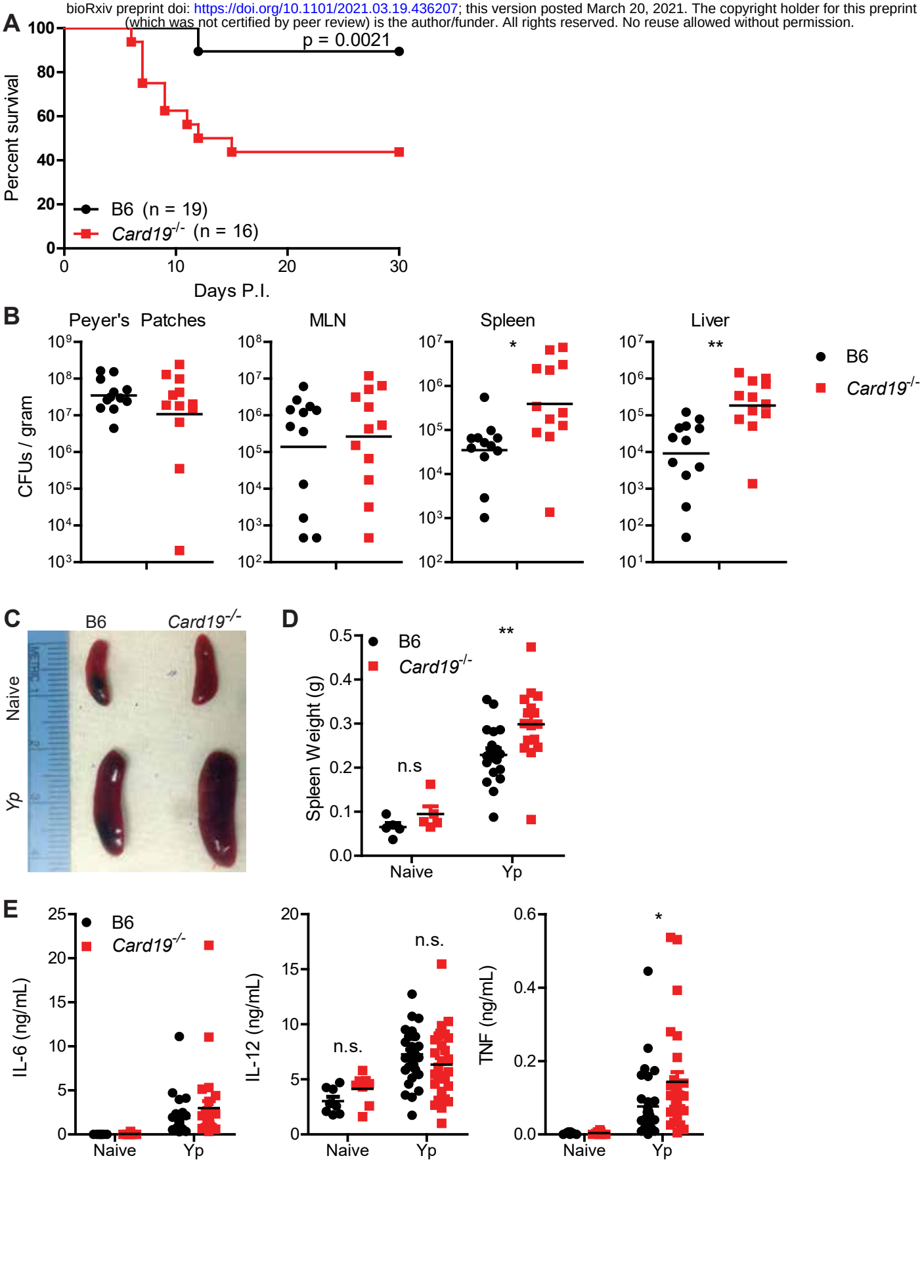

Fig. 7. CARD19 mediates anti-*Yersinia* host defense

(A) Survival of B6 and *Card19*$^{-/-}$ mice following oral infection 10^8 CFUs of strain IP2777 *Yp*. Data are pooled from two independent experiments that each gave similar results. Log-rank (Mantel-Cox) Survival test.

(B) Bacterial CFUs per gram tissue in Peyer's Patches, MLN, Spleen and Liver in B6 and *Card19*$^{-/-}$ mice seven days post-oral infection with *Yp.* Representative of two (PP) or four (MLN, Spleen, Liver) independent experiments. Unpaired Student's *t*-test. ** $p < 0.01$, * $p < 0.05$.

(C) Representative images of naive and *Yp*-infected B6 and *Card19*$^{-/-}$ spleens, seven days post-infection Representative of three independent experiments.

(D) Quantification of naive and infected spleen weights. Data are pooled from three independent experiments with similar results. Naive (n=5), *Yp* (B6 n=19, *Card19*$^{-/-}$ n=16) 2-way ANOVA with Bonferroni multiple comparisons post-test. ** $p < 0.01$.

(E) Serum cytokines from naive and *Yp* infected B6 and *Card19*$^{-/-}$ mice. Data are pooled from four independent experiments with similar results. Naïve (n=8), *Yp* (B6 n=31, *Card19*$^{-/-}$ n=28) 2-way ANOVA with Bonferroni multiple comparisons post-test. * $p < 0.05$, n.s. not significant.

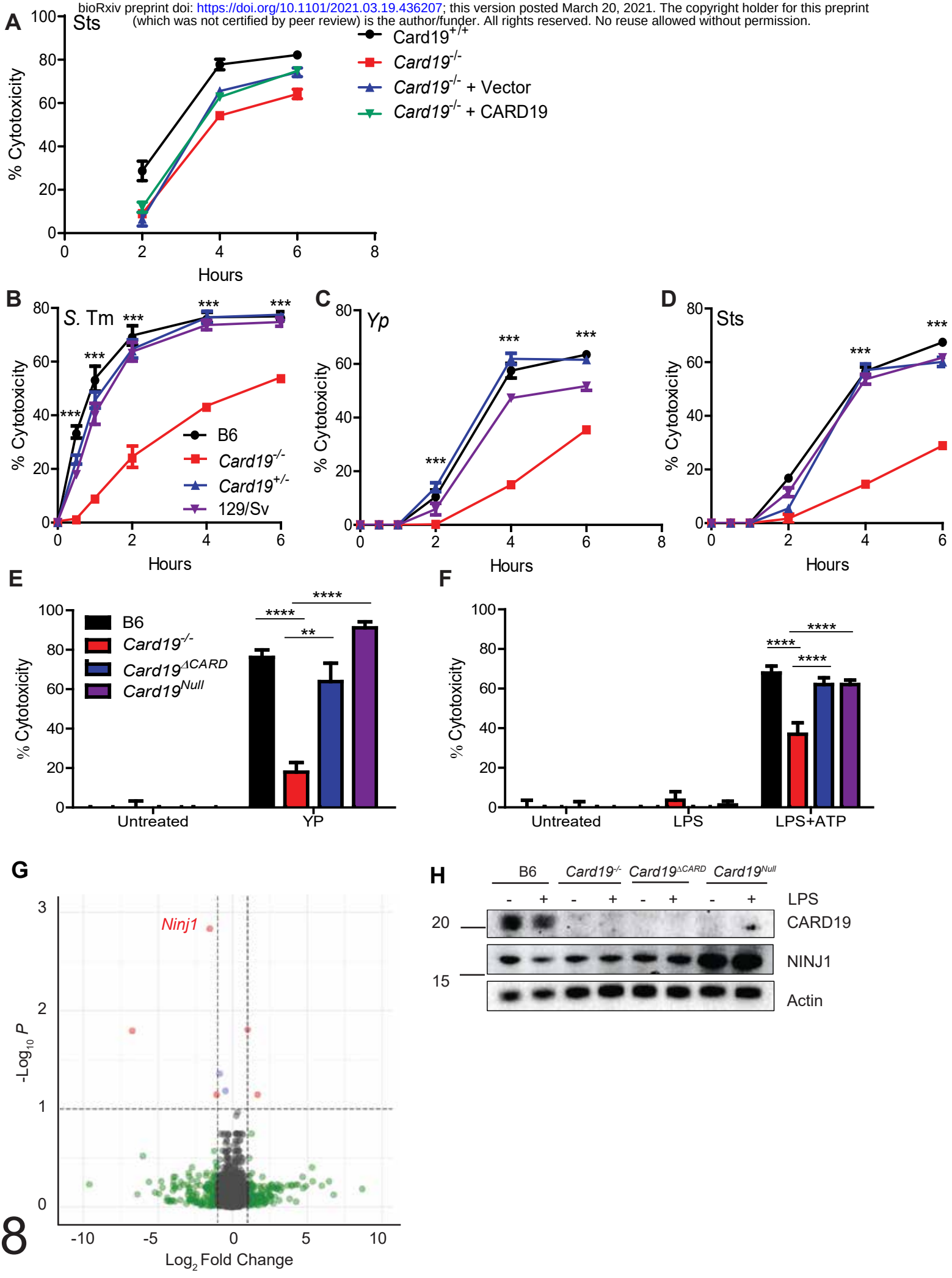

Fig. 8. *Card19*$^{-/-}$ BMDMs regulate cell lysis independently of SARM1 or NINJ1

(A) *Card19*$^{-/-}$ immortalized murine progenitors were stably transduced with CARD19 or empty vector. Mature macrophages derived from untransduced immortalized progenitors *Card19*$^{-/-}$ and Card19$^{+/+}$ and transduced immortalized progenitors *Card19*$^{-/-}$ + Vector and *Card19*$^{-/-}$ + CARD19 were treated with sts. Cell death was assayed by LDH release at indicated time points. Representative of three independent experiments.

(B-D) B6, Card19$^{-/-}$, Card19$^{+/-}$, and 129/Sv BMDMs were treated with (B) *S.*Tm, (C) *Yp* or (D) sts. Cell death was assayed by LDH release at indicated time points. Representative of three independent experiments.

(E,F) B6, *Card19*$^{-/-}$, *Card19*$^{\Delta CARD}$, and *Card19*^{Null} BMDMs were treated with (E) *Yp* or (F) LPS+ATP. Cell death was assayed by LDH release. Representative of three independent experiments. 2-way ANOVA with Bonferroni multiple comparisons post-test. **** $p < 0.0001$ *** $p < 0.001$ ** $p < 0.01$, * $p < 0.05$, n.s. not significant.

(G) Volcano plot from RNA-seq analysis on untreated B6 and *Card19*$^{-/-}$ BMDMs showing differentially regulated genes. Genes whose expression is significantly altered are in red. *Ninj1* is marked.

(H) BMDMs from B6, *Card19*$^{-/-}$, *Card19*$^{\Delta CARD}$, and *Card19*^{Null} mice were primed with LPS or left untreated. Cell lysates were harvested, run on SDS-PAGE and analyzed by western blotting for cleaved CARD19, NINJ1, and Actin (cell lysate loading control).